AD-A173 216 NONLINEAR FRACTURE MECHANICS ANALYSIS WITH BOUNDARY INTEGRAL METHOD(U) SOUTHWEST RESEARCH INST SAN ANTONIO TX T A CRUSE ET AL. 30 MAY 86 SWRI-06-8044 1/2

UNCLASSIFIED AFOSR-TR-86-0862 F49620-84-C-0042 F/G 20/11 NL

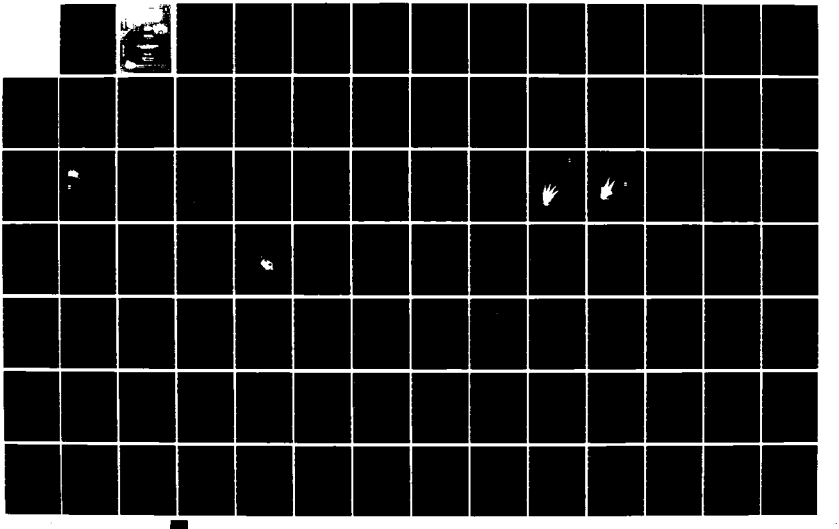

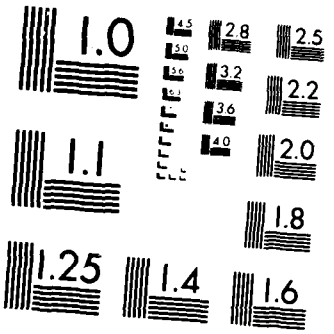

MICROCOPY RESOLUTION TEST CHART
NATIONAL BUREAU OF STANDARDS-1964-A

UNCLASSIFIED

SECURITY CLASSIFICATION OF THIS PAGE

REPORT DOCUMENTATION PAGE

1a. REPORT SECURITY CLASSIFICATION: Unclassified	1b. RESTRICTIVE MARKINGS
2a. SECURITY CLASSIFICATION AUTHORITY	3. DISTRIBUTION/AVAILABILITY OF REPORT: Approved for public release, Distribution unlimited
2b. DECLASSIFICATION/DOWNGRADING SCHEDULE	
4. PERFORMING ORGANIZATION REPORT NUMBER(S): 06-8044	5. MONITORING ORGANIZATION REPORT NUMBER(S): AFOSR-TR- 86-0862
6a. NAME OF PERFORMING ORGANIZATION: Southwest Research Institute; 6b. OFFICE SYMBOL (If applicable):	7a. NAME OF MONITORING ORGANIZATION: Air Force Office of Scientific Research
6c. ADDRESS (City, State and ZIP Code): P.O. Drawer 28510, San Antonio, TX 78284	7b. ADDRESS (City, State and ZIP Code): Bolling Air Force Base, Washington, DC 20332-6448
8a. NAME OF FUNDING/SPONSORING ORGANIZATION: AFOSR; 8b. OFFICE SYMBOL (If applicable): NA	9. PROCUREMENT INSTRUMENT IDENTIFICATION NUMBER: Contract No. F49620-84-C-0042
8c. ADDRESS (City, State and ZIP Code): Bolling AFB DC 20332-6448	10. SOURCE OF FUNDING NOS.

PROGRAM ELEMENT NO.	PROJECT NO.	TASK NO.	WORK UNIT NO.
6110 2F	2302	B2	

11. TITLE (Include Security Classification): NONLINEAR FRACTURE MECHANICS ANALYSIS WITH THE BOUNDARY INTEGRAL METHOD

12. PERSONAL AUTHOR(S): T.A. Cruse and E.Z. Polch

13a. TYPE OF REPORT	13b. TIME COVERED	14. DATE OF REPORT (Yr., Mo., Day)	15. PAGE COUNT
FINAL	FROM 4/2/84 TO 5/30/86	1986 May 30	95

16. SUPPLEMENTARY NOTATION

17. COSATI CODES		
FIELD	GROUP	SUB. GR.

18. SUBJECT TERMS (Continue on reverse if necessary and identify by block number): Fracture Mechanics, two dimensions, elastoplasticity, computational methods, fatigue crack growth, damage tolerance

19. ABSTRACT (Continue on reverse if necessary and identify by block number)

The principal goal of the sponsored research was the development and exploitation of the boundary-integral equation method for fracture mechanics analysis of two-dimensional problems with crack tip plasticity. The formulation approach used was quite unique and was based on a special BIE formulation which explicitly accounts for the presence of the crack in satisfying boundary conditions, and for the elastic problem, satisfying the internal equilibrium conditions. Elastoplastic behavior was successfully added to this special fracture mechanics modeling capability with positive benefits in terms of numerical and theoretical results.

New theoretical developments were achieved as a direct result of the use of a BIE formulation approach. The analytical formulation established limits on the strength of the plastic strain increment singularity. The analytical result demonstrated that the plastic singularity behavior derives from a singular eigenvalue problem of

20. DISTRIBUTION/AVAILABILITY OF ABSTRACT	21. ABSTRACT SECURITY CLASSIFICATION
UNCLASSIFIED/UNLIMITED ☒ SAME AS RPT ☐ DTIC USERS ☐	

22a. NAME OF RESPONSIBLE INDIVIDUAL	22b. TELEPHONE NUMBER (Include Area Code)	22c. OFFICE SYMBOL
Dr. Anthony Amos	202/767-4935	Program Manager

DD FORM 1473, 83 APR — EDITION OF 1 JAN 73 IS OBSOLETE

UNCLASSIFIED

SECURITY CLASSIFICATION OF THIS PAGE

19. (Continued)

a unique form, for the plastic field near the crack tip. At this point, the solution to this singularity formulation is imbedded in the numerical algorithm, as an analytical solution does not seem possible. A new result was achieved for the direct calculation of elastic stress intensity factors for cracks influenced by nonsingular inelastic strains. These problems include residual strain due to welding or elastoplastic notch behavior, thermal strains, etc. As a result of this last result, potentially very important insight has been achieved into the behavior of crack extension into prior plastic zones, due to cyclic loading of the crack. The last major analytical result was the demonstration that the new BIE code could be used as a direct means for calculation of two-dimensional crack weight functions for problems with completely arbitrary geometries, boundary conditions, and internal strain distributions.

Table of Contents

AIR FORCE OFFICE OF SCIENTIFIC RESEARCH (AFSC)
NOTICE OF TRANSMITTAL TO DTIC
This technical report has been reviewed and is approved for public release IAW AFR 190-12.
Distribution is unlimited.
MATTHEW J. KEPPER
Chief, Technical Information Division

Approved for public release; distribution unlimited.

List of Tables

List of Figures

List of Figures
(Cont'd)

Accesion For
NTIS CRA&I
DTIC TAB
Unannounced
Justification
By
Distribution/
Availability Codes
Dist | Avail and/or Special
A-1

1.0 INTRODUCTION

The effect of plasticity on the rate of growth of fatigue cracks is significant for a wide range of problems associated with the damage tolerance assessment of aerospace structures. The range of problems includes crack growth from cold worked fastener holes, crack growth through plasticity due to local notch stresses, crack driving force for thermal gradient fields and welding residual strain fields, small flaw growth in high nominal stress fields, and numerous related problems. These problems have, of course, been analyzed using a variety of approximate analytical or numerical procedures. However, as will be summarized within this report, many of these earlier modeling approaches have involved errors which may significantly affect the predicted fatigue crack growth life of the structure. The current research has resulted in some new and critical insights into this class of problems, while providing a basis for improved modeling of these problems.

The current research makes use of the boundary integral equation (BIE) method, as modified to account exactly for the elastic crack problem. The usual BIE formulation for elastic problems reduces the numerical problem to one of modeling the boundary data, while preserving the complete interior solution of the field equations. In the elastic fracture mechanics problem, the Green's function approach is used wherein the BIE is modified to account for the presence of a stress free crack at an arbitrary location within the structure. The use of the Green's function for the crack eliminates the need to model the boundary of the crack, and provides a complete mathematical description of the elastic strain field within the body, due to the crack.

This clearly contrasts with the finite element method which requires that the crack surface and the interior strains be modeled with some set of interpolation functions.

The BIE method has been successfully modified to account for elastoplastic response by a number of investigators. However, extension of the fracture mechanics model with the Green's function approach has not been previously demonstrated. In order to account for elastoplastic response with the BIE method one must numerically model the interior plastic strain field. In all other ways the elastoplasticity solution uses the standard elastic BIE formulation. The current work reports on the successful extension of the special Green's function formulation for the fracture mechanics problem to the elastoplasticity formulation. Not only has the work resulted in accurate models of crack tip plasticity for a reference problem, but it has shown some important new analytical and numerical results for cracks growing in plastic strain fields.

The second year of the contract effort focussed on the crack extension problem. In the elastic case, a direct solution method for fracture mechanics weight functions was established. The elastoplastic problem considered the extension of the elastic crack into its prior plastic wake. The effects of crack tip overloads on retardation or acceleration through closure and residual stress effects are included. In addition, the elastoplastic BIE formulation was more fully exploited for problems of crack growth in residual strain fields such as weldments.

Some work addressed improvements in a new flat crack BIE formulation for 3D fracture mechanics analysis. The majority of the work on this task was funded by the Internal Research Panel of Southwest Research. However, some analytical formulations, derived from the BIE relations, were achieved under

the current Air Force contract. A report on this 3D formulation completes the technical presentation.

2.0 RESEARCH OBJECTIVES

Generally speaking, advanced aerospace structures have been designed for damage tolerance considerations using elastic fracture mechanics models. Problems associated with residual plastic strains at notches, cold worked fastener holes, weld residual strains, and thermal gradient loading have been modeled using elastic superposition methods along with elastic fracture mechanics models. Crack tip plasticity is involved in all fatigue crack growth problems. Crack tip plasticity dominates the problem of predicting crack growth under spectrum loading conditions where acceleration and retardation effects are important. Finally, the small flaw problem, wherein crack growth rate is apparently accelerated relative to the large flaw problem, cannot be currently explained by elastic fracture mechanics considerations.

The development of improved models for the crack growth problem for the full range of these problems is crucial to improved damage tolerance assessment for advanced aerospace structures. The overall objective for the current research is to provide a new basis for making damage tolerance assessments through numerical modeling of crack tip behavior, including the effects of plastic or other residual strains. The elastoplastic BIE method is the basis for the current effort.

The first goal of the originally proposed program was to extend an existing planar elastic fracture mechanics analysis based on the BIE methodology to the analysis of plastic zones around cracks. The second proposed goal was to establish fundamental results for crack tip elastoplastic behavior, based on a numerical and analytical study of the elastoplastic BIE formulation. The third proposed goal was to establish the credibility of the

elastoplastic BIE formulation relative to the finite element method for refined numerical analysis of the nonlinear fracture mechanics problem, and to apply the capability to important problems of fatigue crack growth modeling for advanced aerospace structures. The goal for the second year of the effort was to extend the research to the problem of modeling crack extension under elastoplastic conditions.

This report summarizes key findings of the current research effort. The next section summarizes the basic two-dimensional elastoplastic formulation and applications. Included in this work are the preliminary applications of the new method to crack extension into prior plastic zones. The next section reports on the use of the new BIE formulation for elastic crack extension. This new result allows for the direct computation of crack weight functions. The last section reports on some recent work, for the 3D BIE fracture mechanics formulation. Some contrast with the 2D formulation is noted. Further work on the 3D problem is expected in the subsequent research program.

3.0 ELASTOPLASTIC FRACTURE MECHANICS MODELING

3.1 Review of the Mathematics

A complete treatment of the elastic formulation for the Green's function BIE model for cracked planar problems is given by Snyder and Cruse [1] and Cruse [2]. The full development of the elastoplastic solution is given by Cruse and Polch [3]. The following summarizes these developments.

The basic BIE formulation for a crack problem, as illustrated in Figure 1, is given as follows

$$C_{ji}u_i(P) + \int_S T^*_{ji}(P,Q)u_i(Q)ds + \int_\Gamma T^*_{ji}(P,\overset{0}{Q})u_i(Q)ds = \int_S U^*_{ji}(P,Q)t_i(Q)ds + \int_\Gamma U^*_{ji}(P,Q)\overset{0}{t_i}(Q)ds \tag{1}$$

In (1) the u_i, t_i terms are the boundary displacement and traction vectors for the modeled problem. The kernel functions (or influence functions) U_{ij}^*, T_{ij}^*, are mathematical entities giving the displacement and traction that are computed on S, Γ for the problem of an infinite body loaded at $p(\mathbf{x})$, $P(\mathbf{x})$† by a set of unit point loads in each coordinate direction. The star on the kernel functions denotes the addition to the point load solution of the terms necessary to provide for a traction free crack at a specified location and orientation in the geometry.

The use of a Green's function for special geometries is well developed in potential theory, as discussed by Greenberg [4]. In the current application we seek to obtain fracture mechanics solutions for the case of traction free

---

†Lower case $p(\mathbf{x})$ is an interior point; upper case $P(\mathbf{x})$ is a boundary point.

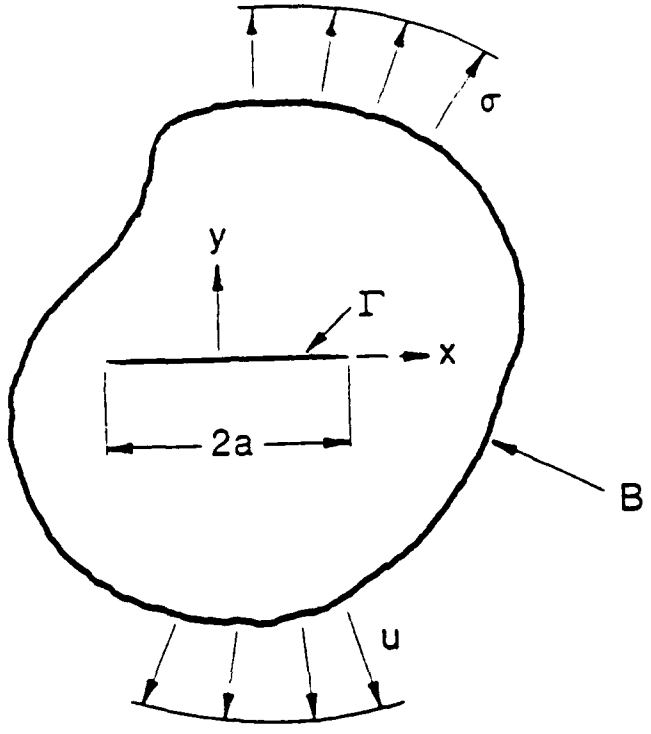

Figure 1. Basic Geometry for Green's Function Formulation

cracks in finite planar bodies. The term with $t_i(Q)$ for $Q \varepsilon \Gamma$ in (1) is therefore zero, as shown. The use of the cracked body Green's function results in the traction kernel also being zero on the crack, viz. $T_{ij}^*(P,Q) \equiv 0, Q \varepsilon \Gamma$, also as shown in (1).

Thus, (1) constitutes the constraint equation that must be satisfied by u_i, t_i on the uncracked portion of the surface. This equation can be reduced to solvable, algebraic form through the use of suitable approximations to the boundary data u_i, t_i. In the current application we use the approximation of piecewise linear interpolations of u_i, t_i as developed by Cruse [2].

The form of (1) for the interior displacement provides a means of direct computation of interior strains, stresses, and stress intensity factors. Simply stated, the interior quantities depend on the totality of boundary data for u_i, t_i through integration of these quantities together with appropriate kernel functions for the cracked plane.

Introduction of inelastic strains (e.g., residual strains due to welding, thermal gradient strains, elastoplastic strains) $\dot{\varepsilon}_{i\ell_A}$ to the BIE formulation †† results in a modification to (1)

$$C_{ji}\dot{u}_i(P) + \int_S T_{ji}^*(P,Q)\dot{u}_i(Q)ds = \int_S U_{ji}^*(P,Q)\dot{t}_i(Q)ds + \int_{\langle A \rangle} \Sigma_{ji\ell}^*(P,q)\dot{\varepsilon}_{i\ell}^A(q)dA \tag{2}$$

The addition of the volumetric (area in 2D) integral in (2) is seen as a correction term to the elastic BIE, (1). The kernel function $\Sigma_{ji\ell}^*$ in this new integral consists of derivatives of the elastic displacement kernel U_{ij}^*, and its form differs for plane stress or plane strain [5].

---

††The dots on the variables denote an increment in the variable.

Equation (2) no longer provides a direct means for computing the boundary data, except when $\dot{\varepsilon}_{ij}^{A}(q)$ is specified. Thus, for elastoplastic response, an additional relationship is needed to compute the plastic strains for (2). The appropriate equation is the interior strain distribution, as written by Cruse and Polch [3].

$$\dot{\varepsilon}_{ij}(p) = \int_S S^*_{kij}(p,Q)t_k(Q)ds + \int_S D^*_{kij}(p,Q)u_k(Q)ds + \int_{<A>} (\Sigma^*_{i\ell m,j} + \Sigma^*_{j\ell m,i})\dot{\varepsilon}^A_{\ell m}(q)dA + E_{i\ell mj}\dot{\varepsilon}^A_{\ell m}(p) \qquad (3)$$

Equation (3) computes the interior <u>total</u> strain increment in terms of the boundary data and the interior anelastic strain increment. For elastoplastic solutions, the unknown data $\dot{u}_j$, $\dot{t}_i$, $\dot{\varepsilon}_{ij}^{A}$ are solved for incrementally and equations (2), (3) are coupled on an iterative basis. The interior inelastic strains are modeled as piecewise constant over ΔA_i area segments in the current study. The full solution algorithm for the elastoplastic case is given in Figure 2. The yield criterion has to be satisfied, giving the amount of total strain that is plastic at each load level. The use of iteration as opposed to a tangent modulus formulation allows us to precompute all of the <u>elastic</u> kernel functions, to invert one of these, and to perform all of the ensuing numerics as matrix multiplications.

3.2 <u>Stress Intensity Factor Computations</u>

The structure of (3) has been investigated by Cruse and Polch [3] for interior points approaching the crack tip. It was found that, for the elastoplastic case where the crack tip strains can exhibit a singularity up to $1/\rho$ (where ρ is the distance from the crack tip), eq. (3) still results in convergent integrals in (2), (3). However, the actual strength of the plastic

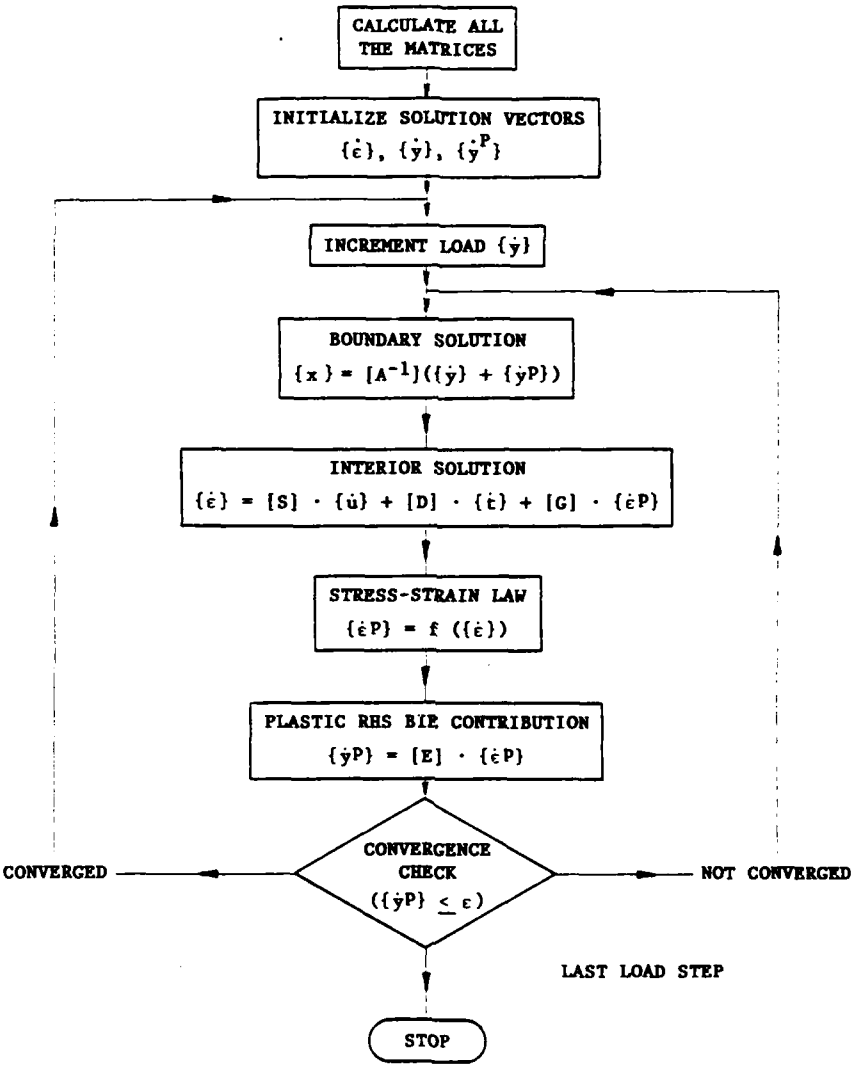

Figure 2. Elastoplastic Solution Algorithm

strain singularity is a function of the work hardening (see Hutchinson [6]) and can only be inferred from the resulting strain distributions after satisfying the flow rule implicit in (3).

The elastic stress intensity factor computation for the BIE formulation using the cracked Green's function results directly from the elastic version of (3). As shown by Snyder and Cruse [1], the kernels in the two boundary integrals in (3) are explicitly dependent on the inverse-square root of the distance of $p(\mathbf{x})$ from the crack tips (+/-a). Further, for the nonsingular distribution of inelastic strains in (3), the volumetric kernel has the same explicit dependence. Thus, for nonsingular, inelastic strains we obtain the following direct, path independent evaluation of the elastic stress intensity factors

$$(K_I,K_{II}) = -\int_s R_i^{I,II}(Q)u_i(Q)ds + \int_s L_i^{I,II}(Q)t_i(Q)ds + \int_A M_{ij}^{I,II}(q)\varepsilon_{ij}^{A}(q)dA \qquad (4)$$

The first two terms in (4) are those previously used by Snyder and Cruse [1] and by Stern, et al. [7]. These are path independent integrals which provide a simple quadrature for computing K_I, K_{II} from any solution for u_i, t_i on a path around the crack, but excluding the crack.

Equation (4) states that nonsingular, inelastic strains modify the elastic K_I, K_{II} values in an equally simple sense of quadrature when these quantities are specified in the volume (area). Some examples of this quadrature for a notch plasticity problem will be discussed below.

In developing eq. (4), it was assumed that the inelastic strains were nonsingular, thus neglecting the crack tip elastoplastic effects. The

additional terms, reflecting the higher order singular behavior, are represented by the incremental elastoplastic strain portion of eq. (3)

$$\dot{\varepsilon}_{ij}^{P}(p) = \int_{<A>} (\Sigma_{i\ell m,j}^{*} + \Sigma_{j\ell m}^{*})\, \dot{\varepsilon}_{\ell m}^{P}(q)\, dA + E_{i\ell mj}\, \dot{\varepsilon}_{\ell m}^{P}(p) \tag{5}$$

As discussed by Cruse and Polch [3], eq. (5) is dimensionally homogeneous for any physical singularity in plastic strain increment as $p(\mathbf{x})+/-a$, but the order of the singularity is not directly solvable from (5).

A considerable number of technologically important problems to the aerospace industry are associated with the use of linear elastic fracture mechanics parameters (i.e., K_I, K_{II}) for problems of limited or localized plasticity. These include predicting K_I for cracks which are undergoing cyclic plasticity resulting in crack closure effects on spectrum crack growth, and cracks growing in the plastic zone of a bolthole subject to high loading or prestressing.

The present research seeks to shed light on some of these problems by presenting a stress intensity factor computation algorithm that can directly and unambiguously model these kinds of limited plasticity effects. For such problems, the solution given in (4) is to be used. The two boundary data integrals in (4) reflect the plastic strain distribution of the crack tip, as well as other anelastic strains through the volume integral in (2). Secondly, the prior plasticity of a notch will affect K_I, K_{II} through the volume integral of those nonsingular strains in (4). The resulting values of K_I, K_{II} are the plasticity corrected elastic stress intensity factors which define the strength of the elastic singularity which dominates the plastic singularity.

The use of this approach is obviously limited to crack tip plastic zones which are contained within the field of the elastic singularity.

3.3 Numerical Solution Algorithm

Application of the appropriate interpolations to the data in eqs. (2) and (3) reduces the integrals to algebraic form. In general, the boundary solution involves an equal number of known (applied) boundary data and unknown data. Letting the unknown data be given by $\{\dot{x}\}$, the product of the known data and its coefficient matrix terms by $\{\dot{y}\}$, and the coefficient of the piecewise constant plastic strains by [E], we obtain from (2)

$$[A]\{\dot{x}\} = \{\dot{y}\} + [E]\{\dot{\varepsilon}^P\} \tag{6}$$

Similarly, taking [S] and [D] to be the elastic coefficient arrays of the boundary data, and [G] to be the elastic coefficient array for the plastic strain, then eq. (3) becomes

$$\{\dot{\varepsilon}^T\} = [S]\{\dot{t}\} + [D]\{\dot{u}\} + [G]\{\dot{\varepsilon}^P\} \tag{7}$$

The strain superscripts in (6) and (7) refer to total (elastic plus plastic) and plastic values, while the dots imply that all of the variables are to be interpreted in terms of their incremental evaluation.

The present BEM algorithm makes use of the Huber-Mises-Hencky yield condition and associated flow rule. Elastic, perfectly plastic material response was modeled throughout this study, but the code allows for a multi-piecewise-linear definition of a general stress-strain curve.

Following the approach adopted in the ADINA code, each increment in total strain is divided into subincrements (Bathe [8]). The number of subincrements

is selected to minimize the error in the deviatoric stress change within the strain increment. The stress increment for a given iterate of increment in plastic strain is then obtained by an Euler forward integration of the flow rule, according to

$$\{\sigma_{\substack{\text{CURRENT}\\\text{LOAD}}}\} = \{\sigma_{\substack{\text{PREV}\\\text{LOAD}}}\} + \int_{\epsilon^T_{\text{PREV LOAD}}}^{\epsilon^T_{\text{CURRENT LOAD}}} [C^{EP}]d\epsilon^T \tag{8}$$

In eq. (8), the elastoplastic matrix relating the subincrements in stress and total strain is given for plane strain by

$$d\sigma_{ij} = 2G[\delta_{im}\delta_{jn} + \frac{\nu}{1-2\nu}\delta_{mn}\delta_{ij} - \frac{S_{ij}S_{mn}}{2J_2(1 + H/3G)}]d\epsilon^T_{mn} \tag{9}$$

The current state of deviatoric stress, S_{ij}, and second invariant of deviatoric stress, J_2, is updated within the subincremental integration of (8). The tangent modulus, H, is taken as the slope of the effective stress-effective plastic strain curve, at the current level of effective stress.

Figure 2 summarizes the current iteration algorithm for the solution of eqs. (6,7). The coefficient arrays [A], [S], and [D] depend solely on the elastic constants of the material and the boundary shape. Thus, they are computed once and stored. The [A] matrix is inverted prior to storage. The interior arrays [E] and [G] are also dependent solely on the elastic constants and the interior element modeling. These are also computed once and stored. Note again that only that portion of the interior expected to be inelastic

need be modeled. The expense of generating [E] and [G] for crack problems dictates that such limited volumetric modeling be employed.

In the first iteration at a given load step, the plastic strain increment in Figure 2 is taken from the last load step. The boundary solution then responds, in an elastic manner, to the increase in loading. Estimated interior total strains are then calculated. Based on the new total strain increment, the interior stresses and plastic strains are computed based on satisfying the yield condition through eq. (8). The plastic strain increment is then updated in both eqs. (6,7) for a recalculation of the boundary and interior solutions.

Absolute convergence of the strain solution within each element is required for the iteration process used. That is, the maximum difference between successive iterates of the plastic strain correction term (second term on the right hand side of eq. (6)) is not allowed to exceed a user-specified tolerance. This tolerance has been selected on the basis of its ability to relate directly to the amount of the displacement increment. A number of numerical experiments with tolerances ranging over 10^{-6} to 10^{-9} were conducted to test the sensitivity of the results to this value. It was found that the errors in the displacements, for a simple uniform stress test case, were of the order of the tolerances specified. A decrease in the tolerance by an order of magnitude generally resulted in a doubling of the number of iterations required to achieve convergence. A value of 10^{-7} was used for the notch problem and a value of 10^{-9} was used for the fracture mechanics problem, in order to account for the higher strain gradient.

3.4 Numerical Results

The computer program has been verified on two example problems. The first is a plate with perforations, previously solved by Haward and Owen [9]

using finite elements and resolved by Telles [10] using the BEM. This example served the basic purpose of validating the current code and provided a basis for some numerical experimentation. The second problem is a fracture mechanics problem of a center cracked plate loaded in tension. The plastic strain results are compared to ADINA results using a singular finite element model.

The geometry for the first problem is shown in Figure 3. Plane strain conditions are applied for all three of the analyses and the material is taken to be elastic-perfectly plastic. The appropriate constants are $E = 42. \times 10^3 MN/m_2$, $\sigma_y = 105.\ MN/m^2$, $\nu = 0.33$. The one loading condition considered was uniaxial tension, applied by prescribing displacements at the edges of the plate section. The piecewise linear plastic strain BEM mesh of Telles is shown in Figure 3; the FEM quadratic isoparametric element mesh used by Haward and Owen is shown in Figure 4. The current BEM mesh, using piecewise constant plastic strains, is shown in Figure 5.

Figure 6 plots the numerical results in terms of the amount of force required versus the applied displacements. Table 1 summarizes the numerical force-displacement data. All three model results show excellent agreement, given the disparity in modeling strategies. The predicted limit load for the current study differs from the other two by less than 2%. The difference is attributed to the use of constant strain elements. Limit load is obtained when the centroidal value of stress in the last ligament element yields, a condition that will occur below the load for yielding the last physical ligament ahead of the notch. The plastic zones are shown in Figure 7 for various load levels.

The current BEM code was tested for a range of load increments in a deliberate attempt to create numerical instability. The numerical results

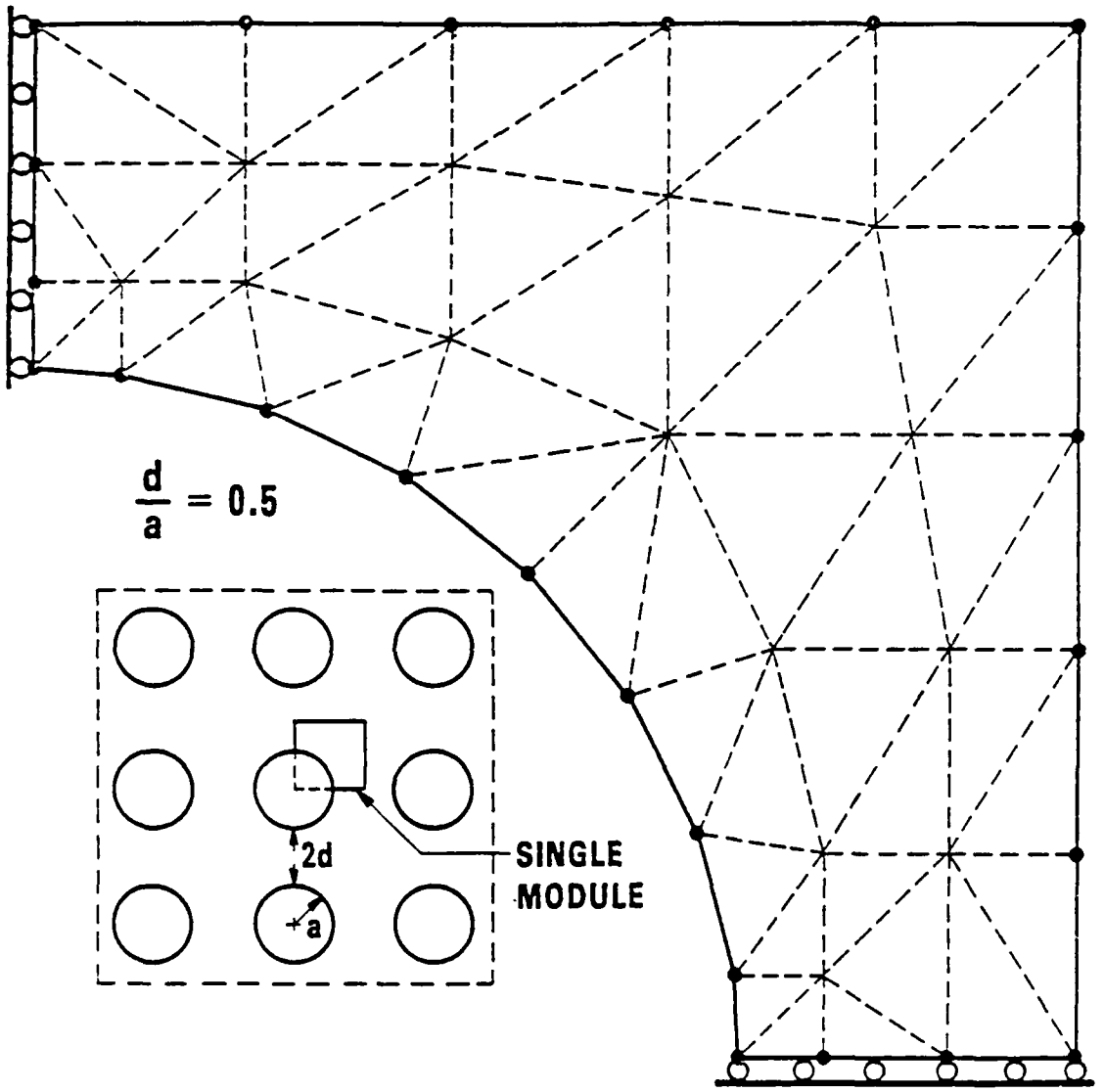

Figure 3. Perforated Polystyrene Plate and BIE Discretization Used by Telles (1983)

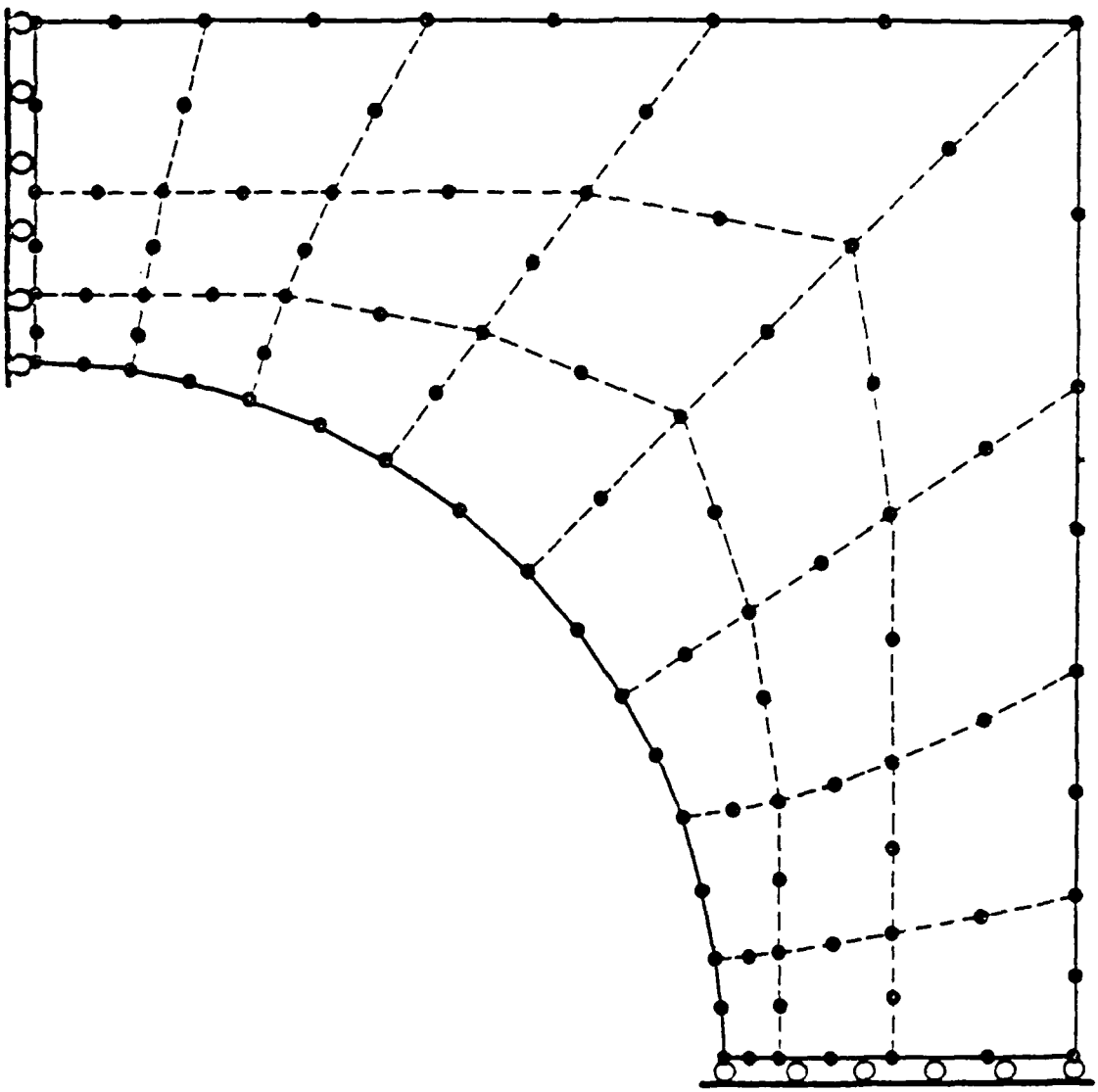

Figure 4. Quadratic Isoparametric Finite Element Mesh Used by Haward and Owen (1973)

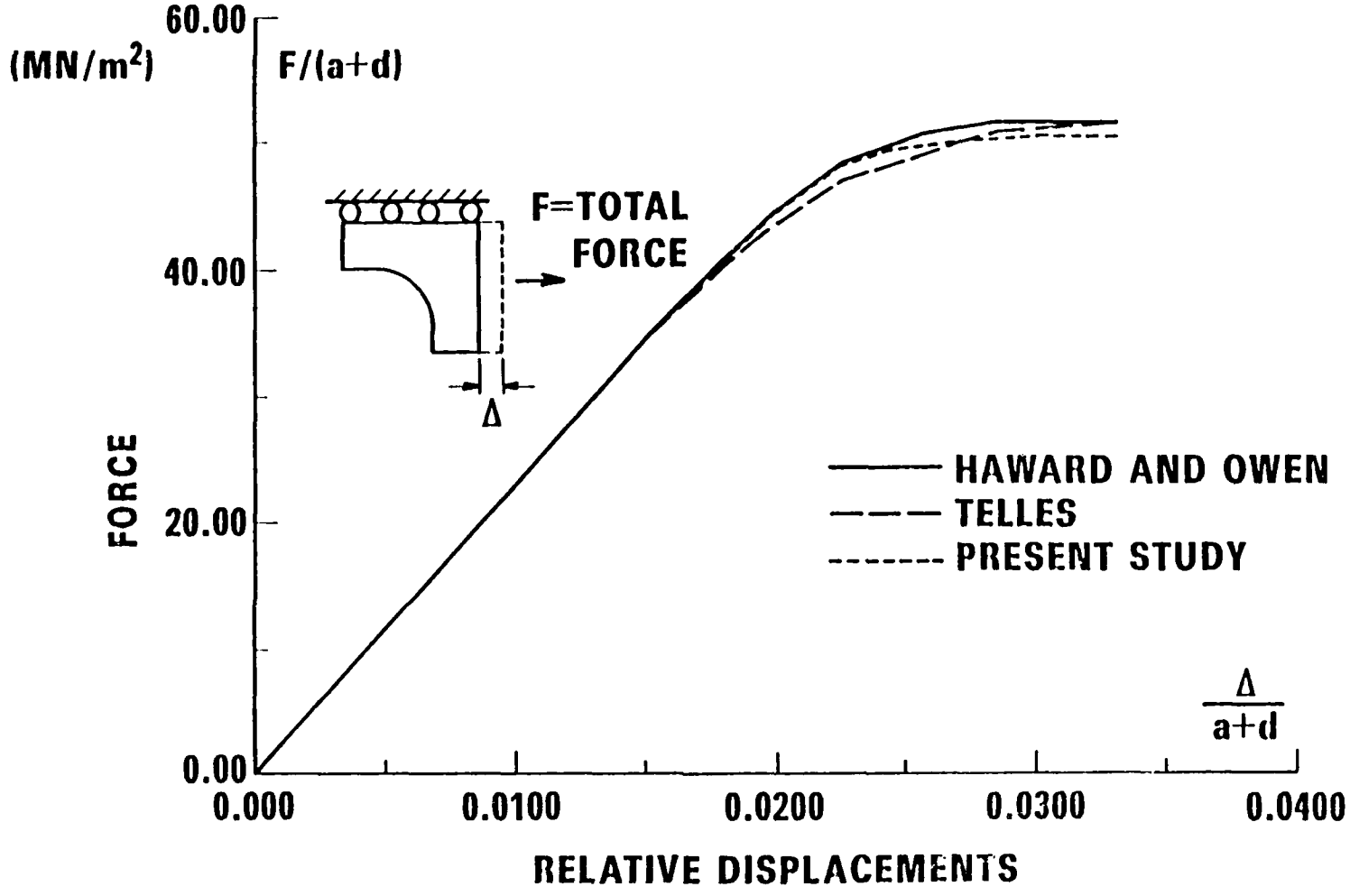

Figure 6. Results of the Polystyrene Plate Problem

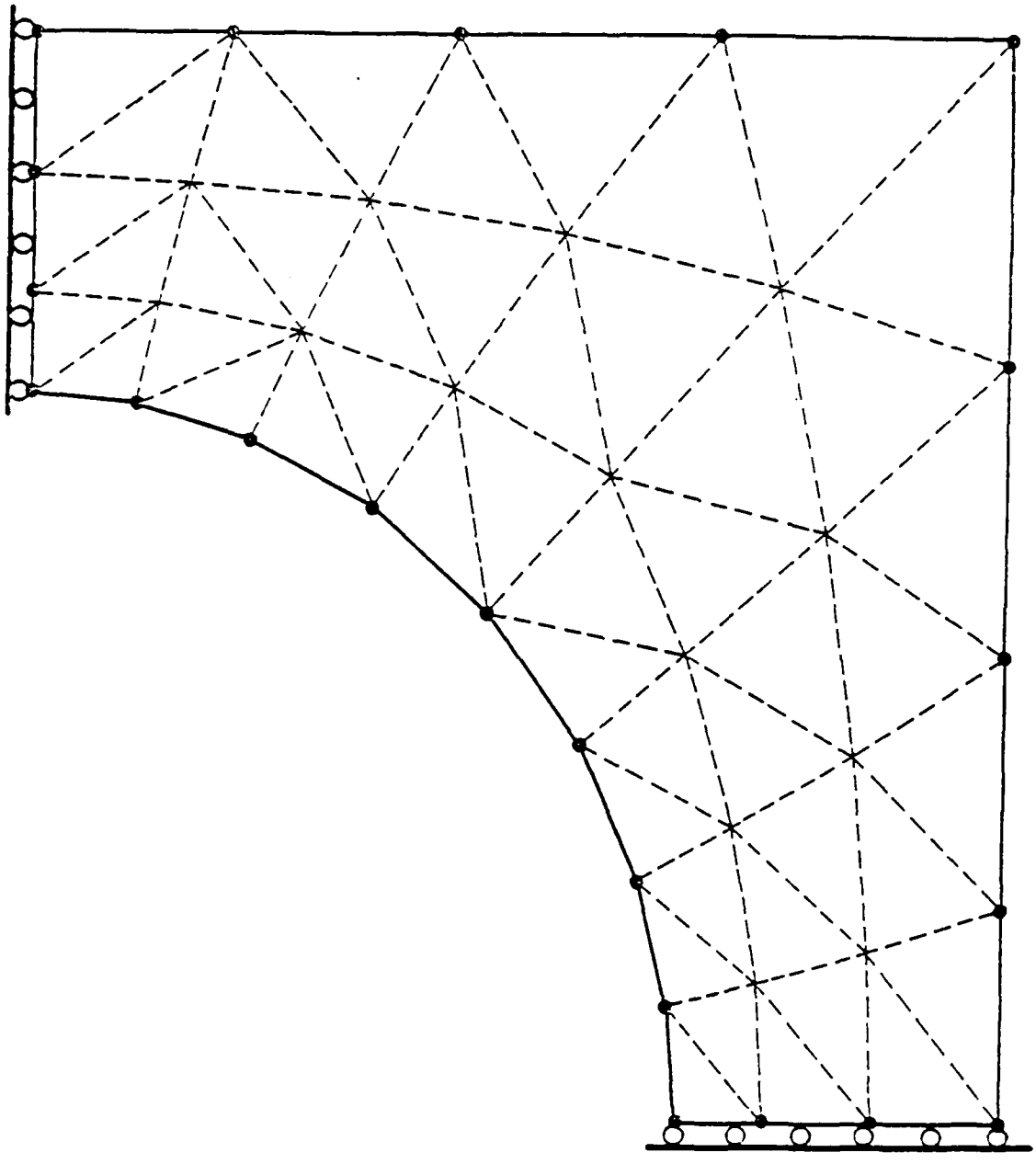

Figure 5. BIE Discretization Used in the Present Study

Table 1.

Numerical Results of the Polystyrene Plate Problem

PCP - Uniaxial Stretch

Load Case	Load %	Displacement ($A \times 10^{-3}$)	Force (F)	$\frac{\Delta}{a+d}$ (x 10-z) [%]	F/(a+d)
1	.50	4.5	10.3576	1.50	34.525
2	.55	4.95	11.3259	1.65	37.753
3	.60	5.4	12.2459	1.80	40.820
4	.65	5.85	13.1047	1.951	43.682
5	.70	6.3	13.8412	2.10	46.137
6	.75	6.75	14.4610	2.25	48.203
7	.80	7.2	14.7765	2.40	49.255
8	.85	7.65	14.9091	2.55	49.697
9	.80	8.1	15.0009	2.70	50.003
10	.95	8.55	15.0650	2.85	50.217
11	1.00	9.0	15.1112	3.00	50.371
12	1.05	9.45	15.1412	3.15	50.471
13	1.10	9.9	15.1412	3.30	50.471

The ultimate strength = 50.471 MN/m^2

a, d defined in Figure 2

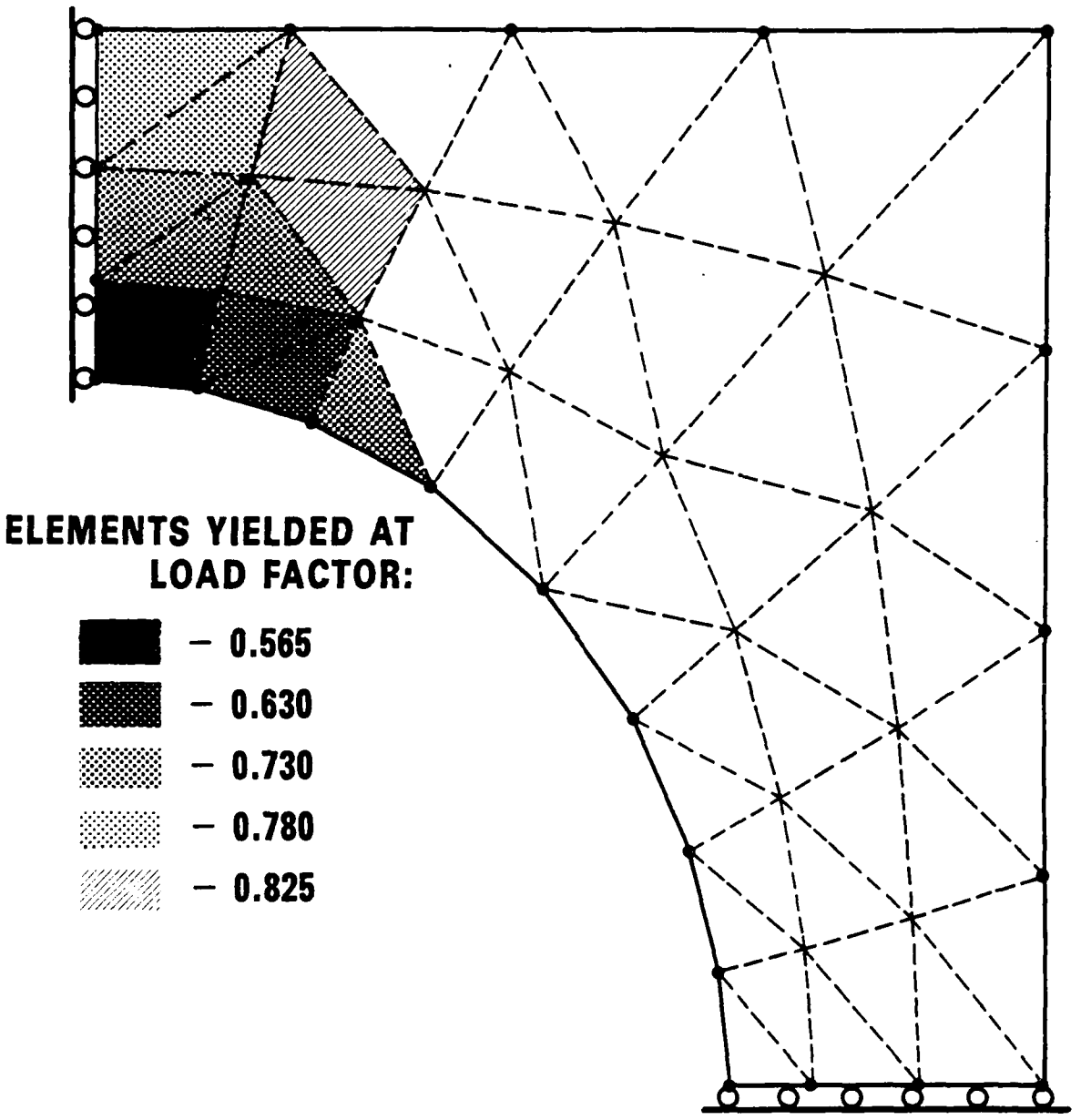

Figure 7. Growth of the Plastic Zone

plotted in Figure 6 were generated using an incrementation scheme resulting in a single element yielding at a time. The BEM results required about twenty iterations per load step to fully converge. The worst case was one load step to the maximum displacement. The solution converged in 45 iterations and agreed with the other limit load results within 0.2%. The maximum deviation in calculated plastic strains was 10% in the last element to yield.

The second example is a center-cracked plate loaded in tension. The total width of the plate is 8 units, with a crack size of 2 units. One quarter of the geometry was modeled using ADINA, as shown in Figures 8 and 9. Extremely fine resolution of the crack tip elements was taken in order to minimize the error in the finite element solution. The elastic stress intensity factor for this finite element model, using the crack opening displacement at the quarter-point node, was in error relative to handbook values by about 2%.

The BEM mesh corresponding to the local finite element scale is shown in Figure 10. The elastic BEM stress intensity factor results were indistinguishable from the handbook results. The FEM/BEM meshes were selected so as to provide about three decades of plotting data in terms of crack tip distance. The maximum size of the plastic zone was limited solely for convenience in the current study.

Plane strain conditions were used for both of the models. The elastoplastic material constants used were $E=2.037\cdot10^5 MN/m^2$, $\sigma_y=3.452\cdot10^2 MN/m^2$, and $\nu=0.27$.

The ADINA crack tip model used quadratic, isoparametric finite elements with nine interior strain integration points. The BEM model used constant strain triangles throughout. As noted above, both meshes were identical in the crack tip region. The ADINA model used one layer of collapsed quadratic elements adjacent to the crack tip. This approach induces a (1/r) type of

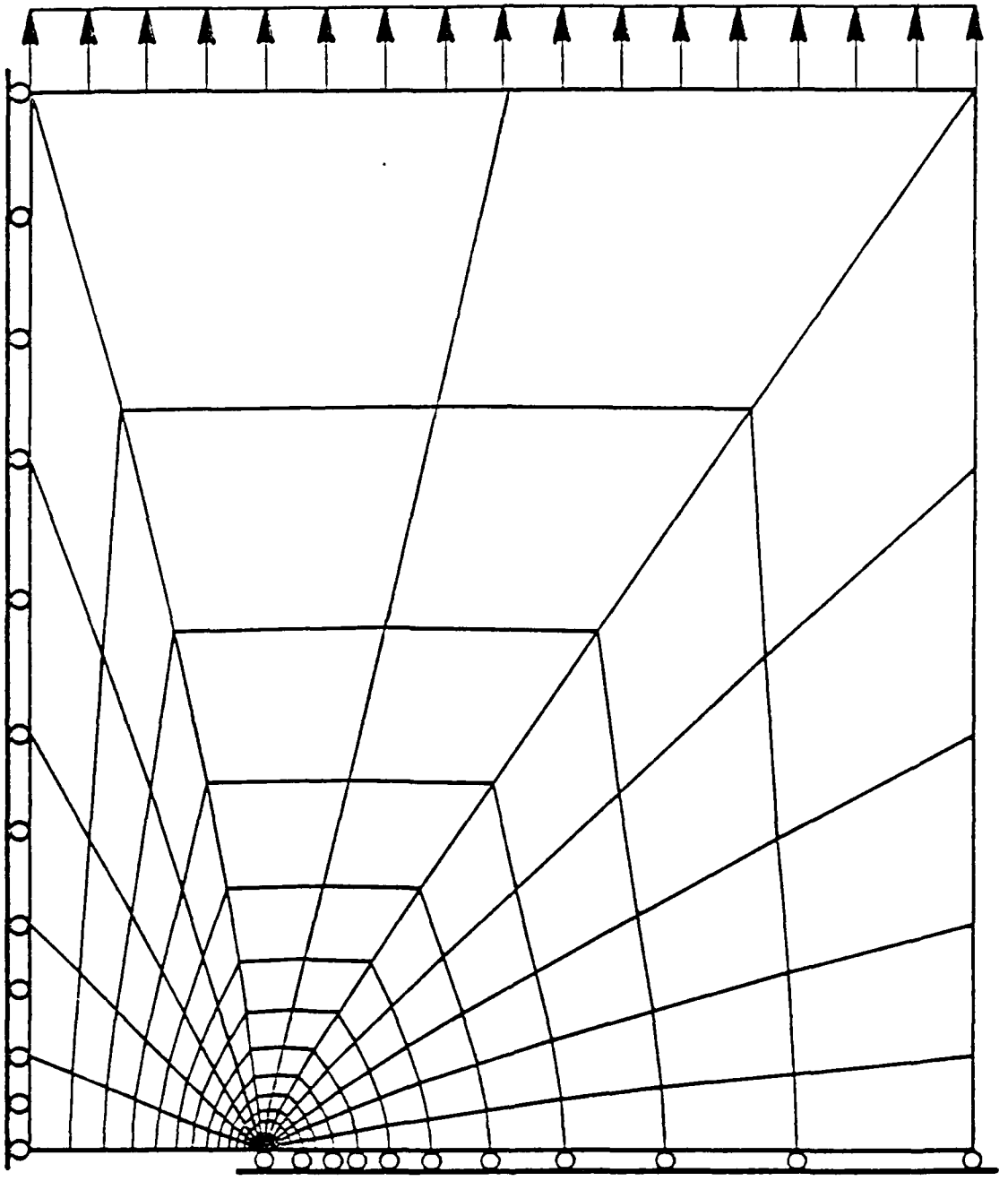

Figure 8. Finite Element Mesh of the Center-Cracked Plate

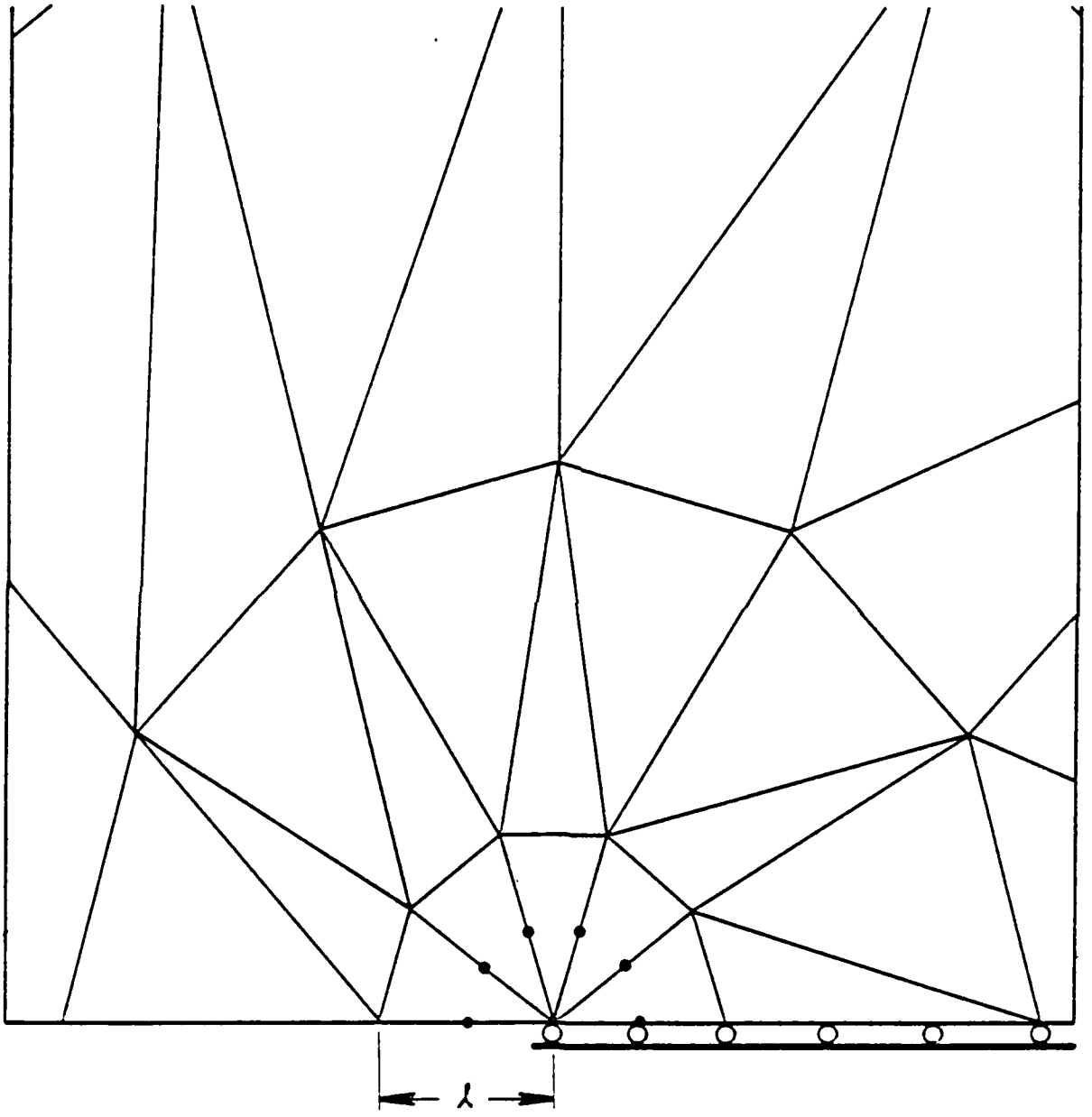

Figure 9. Finite Element Modeling of the Crack Tip Vicinity with Singular Elements (ℓ/a = 0.001)

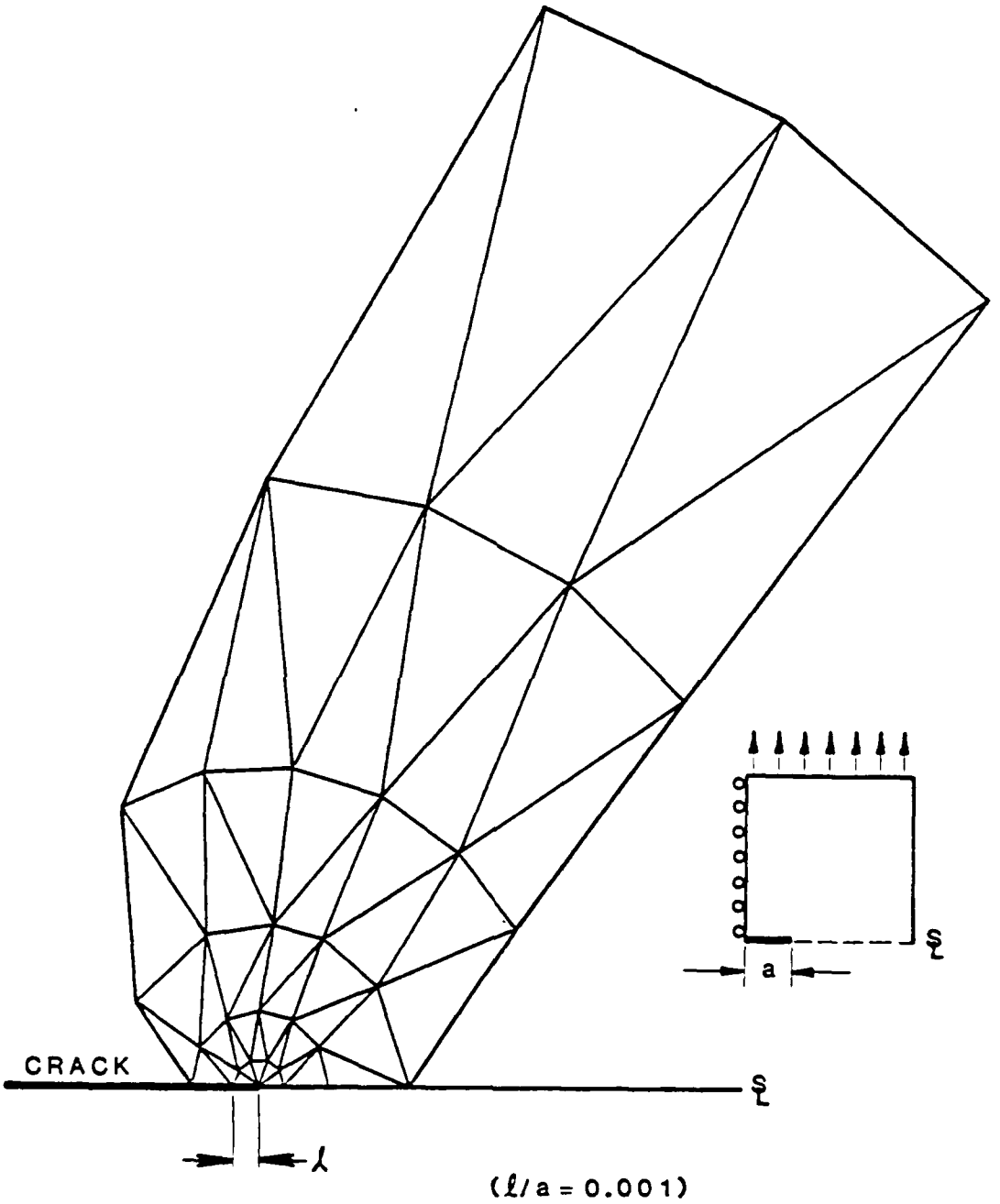

Figure 10. Internal Plastic Strain Elements for the Boundary Integral Equation Modeling of the Crack Tip Vicinity ($\ell/a = 0.001$)

singularity in the displacement gradient within this first layer of elements. No singularity modeling is used in the BEM plastic strain distribution.

Loading history was identical for both models and spans the range of load factors of 0.0310 to 0.2075. A value of 1.0 corresponds to yielding of the whole plate. A total of 68 load steps was used for both models. The load steps satisfy the conditions of Larsson and Carlsson [11]. Simply stated, these conditions require that at most one element becomes plastic at each load increment, and that the load increment should be smaller than 1% of the load corresponding to $K_{Imax}=\sigma_y \cdot \sqrt{a}$. The range of load factors has been chosen as the range to go from yielding the innermost element to yielding the outermost element.

ADINA failed to converge for the first step until the stiffness reformulation (BFGS) procedure was used. After the first load step (requiring 20 iterations) the ADINA algorithm with reformulation generally converged with five iterations. The BEM algorithm, using elastic "stiffnesses," converged in ten to fifty increments at each load step with the higher numbers occurring at the higher load levels. The total computer time for the two models was essentially the same, although the BEM calculations are cheaper per load step. A higher final load level or cyclic loading would yield a benefit to the BEM model, even though the current BEM code is not yet optimized for these calculations.

The crack tip plastic strain distribution results are shown in Figure 11 for two of the computed load levels. The data are taken from points distributed near, but not on, a line at an angle of about 85° to the plane of the crack. This angle corresponds to the line of maximum equivalent elastic strain. The jaggedness of the curves is mostly due to the use of triangular

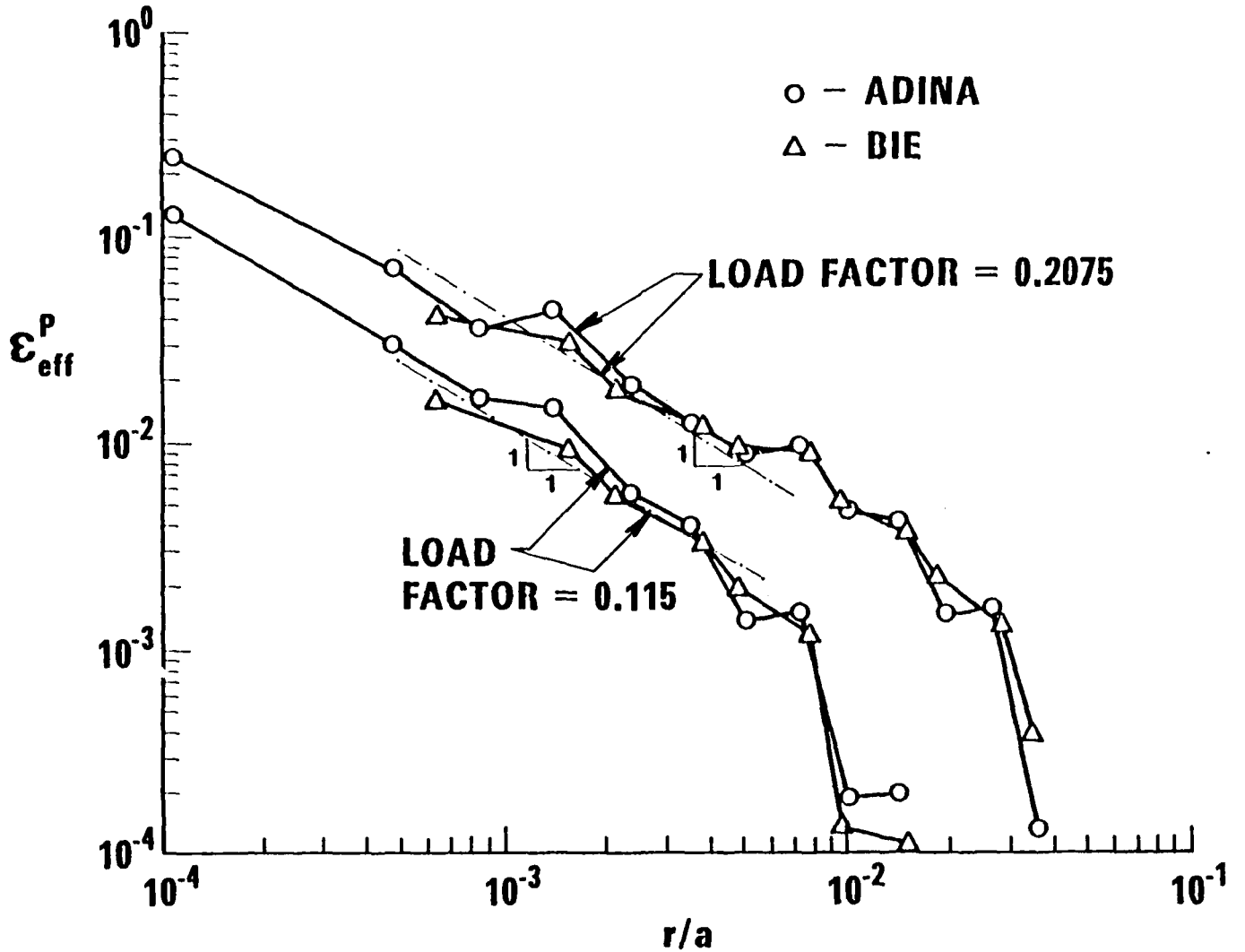

Figure 11. Effective Accumulated Plastic Strain Distribution

elements, as well as to the points having different angular locations. The data is plotted in terms of the centroidal value of plastic strain. The innermost row of finite elements has three sampling points radially, which accounts for the smaller radius plotted for these results. The numerical results from ADINA show a tendency for a spurious peak in plastic strain increments in the second row of elements. This peak is no doubt induced by the lack of a singularity-transition element in the current study.

It is significant to find that the numerical results are in such good agreement. This confirms the accuracy of the BEM algorithm for piecewise constant plastic strains. The BEM results do not show the strength of the plastic singularity as strongly in the first row of elements as do the finite element results, with the imbedded 1/r singularity in displacement gradient. However, both sets of results strongly indicate that the plastic strain for localized plasticity possesses the same 1/r singularity that is associated with fully developed plasticity for the case of zero strain hardening. Clearly, the presence of the underlying elastic singularity field plays an important role in enhancing the modeling accuracy for crack tip plasticity.

Figures 12 and 13 show the progressive development of the plastic zone up to the maximum modeled load. It is to be emphasized that the current study was intended to confirm the accuracy of the new BEM algorithm for elastoplastic fracture mechanics analysis, and not study extensive plasticity response at the crack tip. For this reason the current results were not carried beyond the load level shown. There is no inherent limit to the load level that can be modeled with this BEM algorithm.

3.5 Crack Extension

The numerical implementation of the elastoplastic fracture mechanics algorithm in this section report focuses on problems for which the plasticity

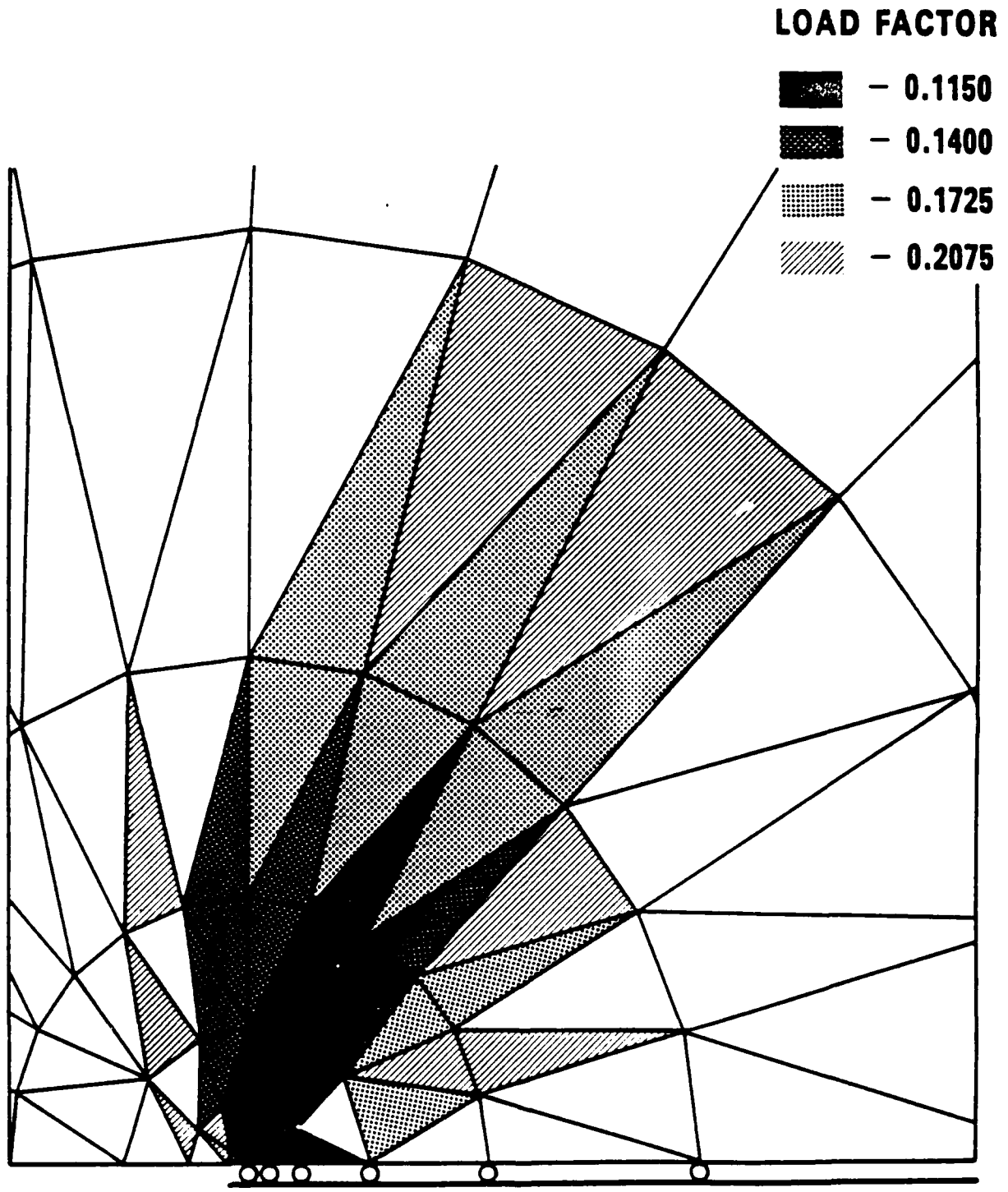

Figure 12. Growth of the Plastic Zone (ADINA)

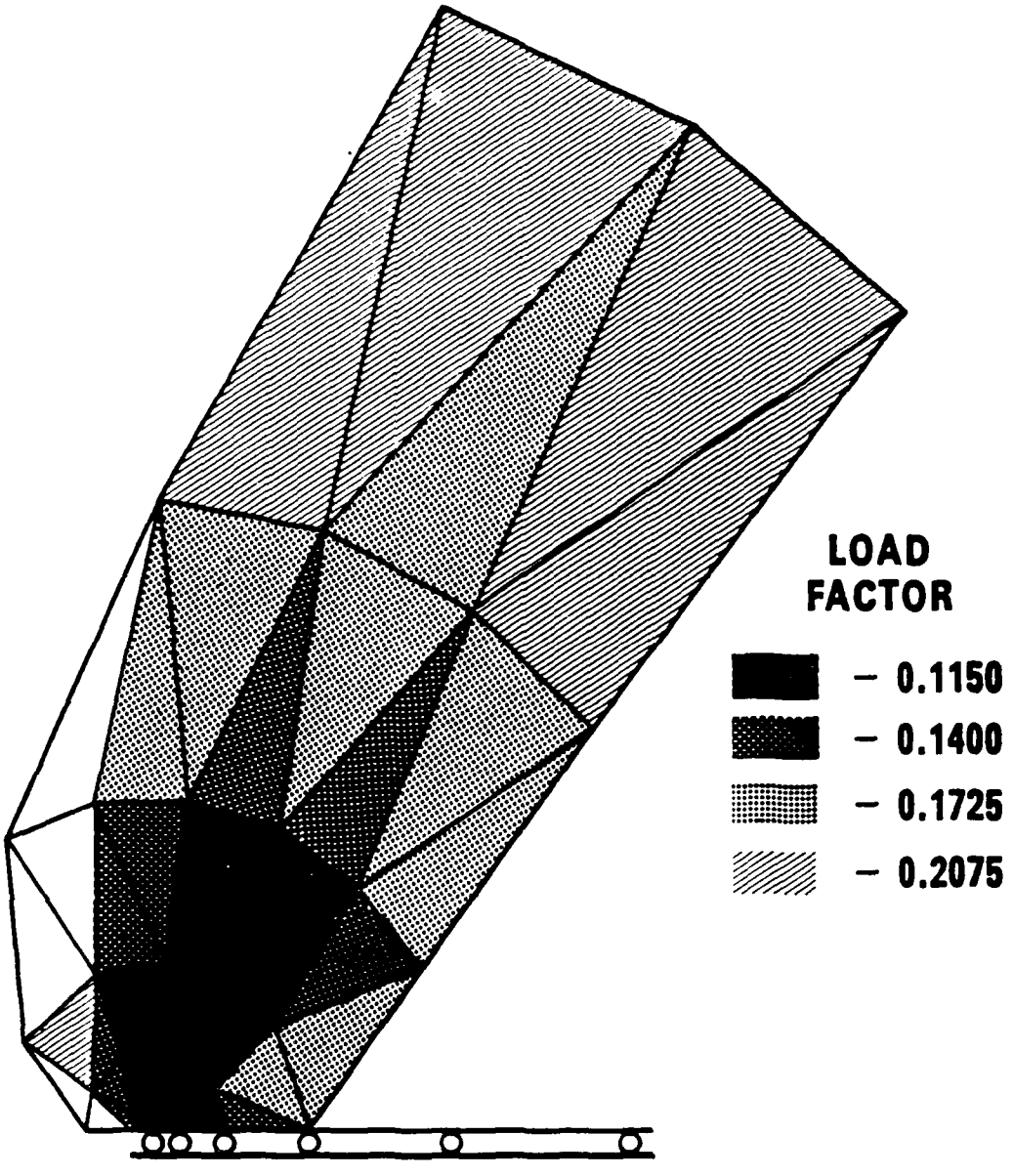

Figure 13. Growth of the Plastic Zone (BIE)

modified, stress intensity factor in eq. (4) is useful. In matrix form, this becomes

$$K_{I,II} = \langle R \rangle \{u\} + \langle L \rangle \{t\} + \langle M \rangle \{\varepsilon^P\} \qquad (10)$$

These problems consist of elastic cracks in the presence of plastic strains due to welding and to yielding of notches.

The first problem was selected to validate the stress intensity factor algorithm for prior plasticity for any residual or thermal strain field. The geometry selected is a simple tension specimen with the boundary and internal mesh shown in Figure 14. The mesh arrangement was selected solely for convenience, as it is used as a portion of a later mesh. The specimen was loaded to 110% of the yield stress for a bilinear material response. This induced a uniform plastic strain throughout the specimen.

The next step in the validation of eq. (10) was to introduce a crack, done along the bottom of the mesh as shown. The residual boundary solution corresponding to the residual internal strains is computed for the cracked case by eq. (6). Next, the internal strains for the residual boundary and internal variables are computed from eq. (7). In the case of the test problem, eq. (6) produced the uniform displacements compatible with uniform residual strains; eq. (7) computed internal strains equal to the residual strains.

The elastic stress intensity factor for the problem was then computed for the residual boundary terms computed from eq. (6). If there were further changes in the residual strains due to unloading plasticity, these would modify the elastic strain intensity factory through the appropriate term in eq. (10). As required for this simple case, the residual stress intensity

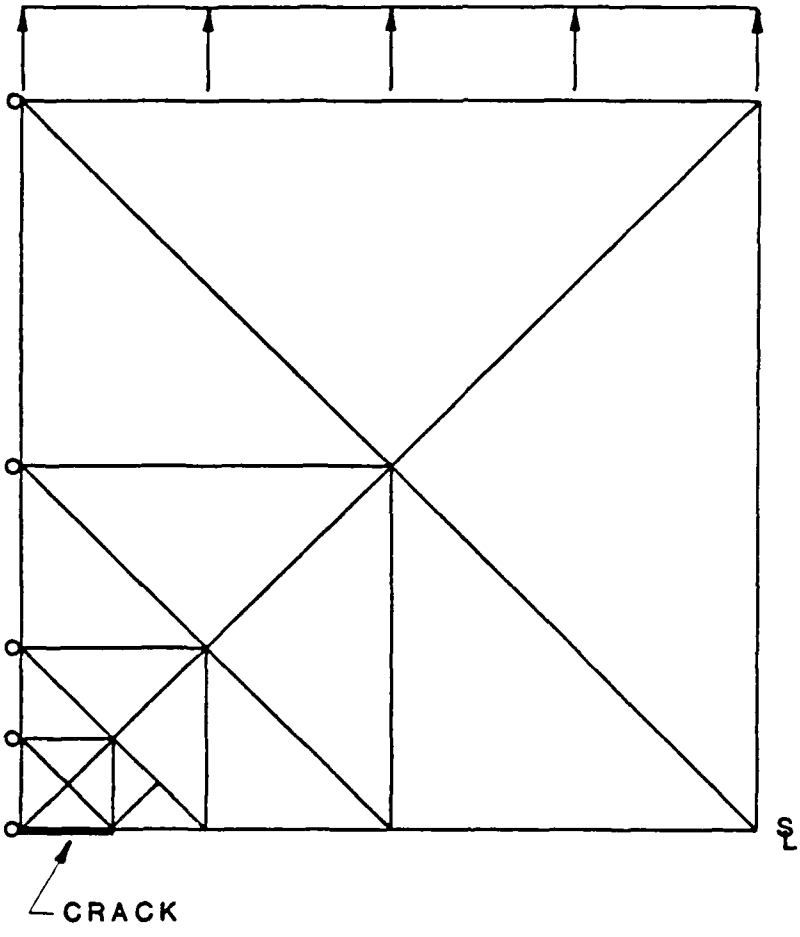

Figure 14. Test Problem for Uniform Strains

factor was zero. The residual values in the first and third terms in eq. (10) cancel each other to within computer accuracy.

Figure 15 shows the residual stress in a large plate containing a simulated weld bead. The weld is simulated by a narrow (b/W = 1/400) strip of material with plastic strains equivalent to 100 ksi elastic strains in an infinite sheet. Both plane strain and plane stress solutions were used. The plastic strains simulate the behavior of material which is heated to yielding in a confined region, and then allowed to cool. The slight accommodation of the plate to equilibrate the residual, welding stresses is seen in Figure 15.

The BIE/CRX analysis was used to obtain K-solutions for various central crack sizes for cracks transverse to the weld bead. The only reason for this configuration is to be able to compare the numerical results to an exact solution for the residual stresses in Figure 15.

The approach taken is to solve eq. (6) to establish the boundary solution corresponding to the residual strains. Two triangles were used to integrate the plastic strains in eq. (6,10); a single quadrilaterial element would also suffice.

The results of K(a) are compared to the analytical results using an influence function approach [12] in Figure 16. The agreement is essentially exact, as expected. The volume integral in eq. (10) contributes the bulk of the K-solution, as the boundary displacements associated with the weld plastic strains are very localized.

The algorithm in eq. (10) is therefore seen to be a very powerful solution for residual plastic strains for geometries without known Green's functions or influence functions. Further, by slight reformulations of the volume terms, other volumetric strains such as thermal strains or body force strains can be analyzed in the same manner.

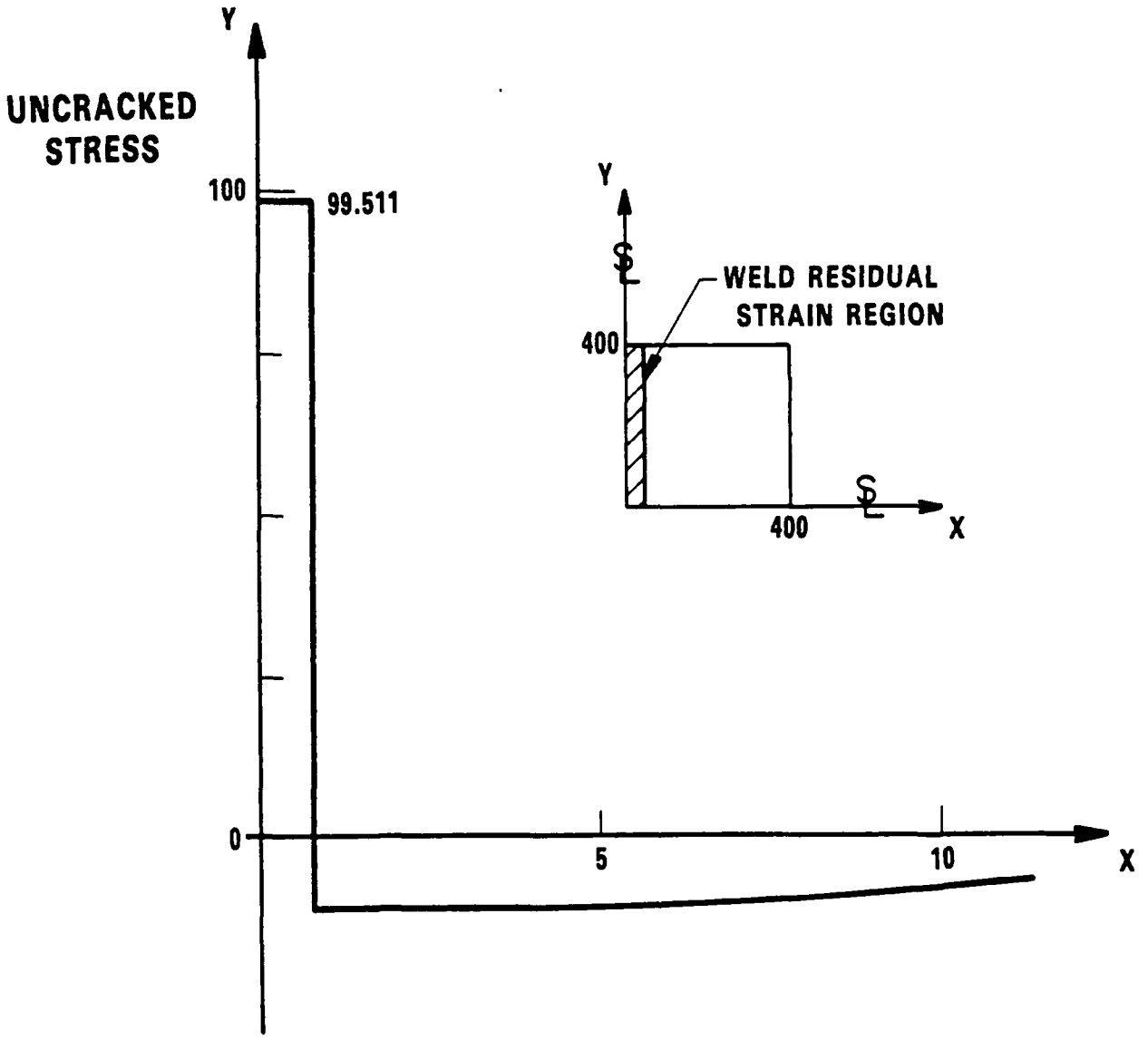

Figure 15. Simulated Residual Stresses Due to Welding

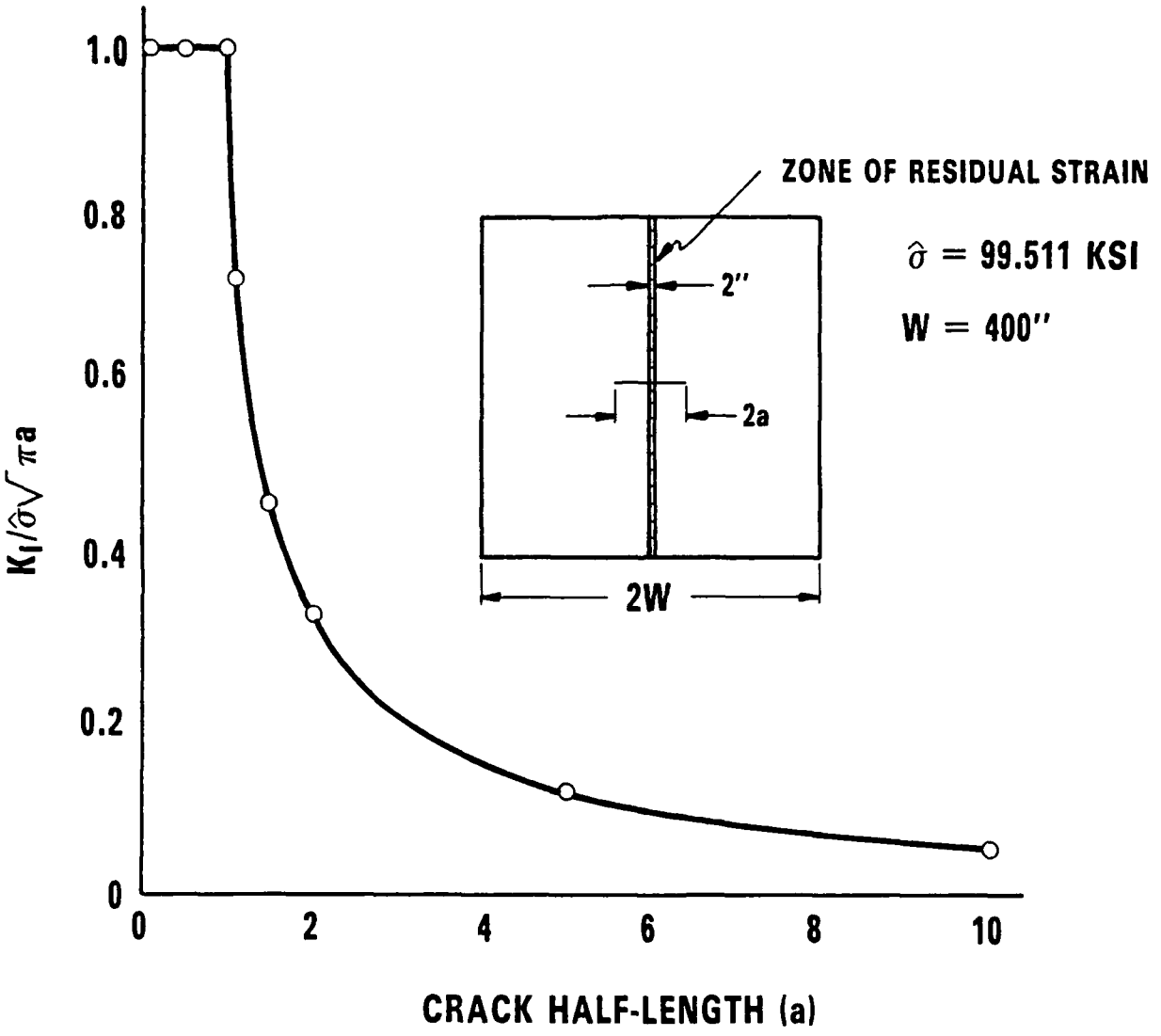

Figure 16. Stress Intensity Factor Distribution for Center Crack in Simulated Welded Plate

An important engineering application of this approach is the calculation of K(a) for cracks at notches (holes, fillets, etc.) which have plastic strains due to overloads, or cold working. To simulate this problem, a bolt hole specimen was modeled as shown in Figure 17. The plate was loaded in plane strain to 80% of the net section plane strain yield stress (F_{ty} = 55.8 ksi). Figure 18 shows the progressive development of the plastic strain, computed by the BIE/CRX program with zero crack length.

An elastic crack was then simulated for a/R = 0.05, 0.50. The solution, as before, requires an equilibrium adjustment to account for the crack in the boundary solution (6), and a K-calculation from eq. (10). In this case, the boundary terms in (10) contributed a significant portion of the solution.

Table 2 presents the elastic and plasticity-modified stress intensity factors for the two crack lengths. The approach used is to calculate K(a) from eq. (10) at no load. Table 2 gives the values of K(a) at no load and full load through an addition of the elastic result to the no load solution. The results clearly demonstrate how notch plasticity causes substantial crack closure (K(a) < 0), thereby reducing the stress intensity factors at full load. Such retardation effects due to residual stress have been previously modeled with influence function approaches [13,14].

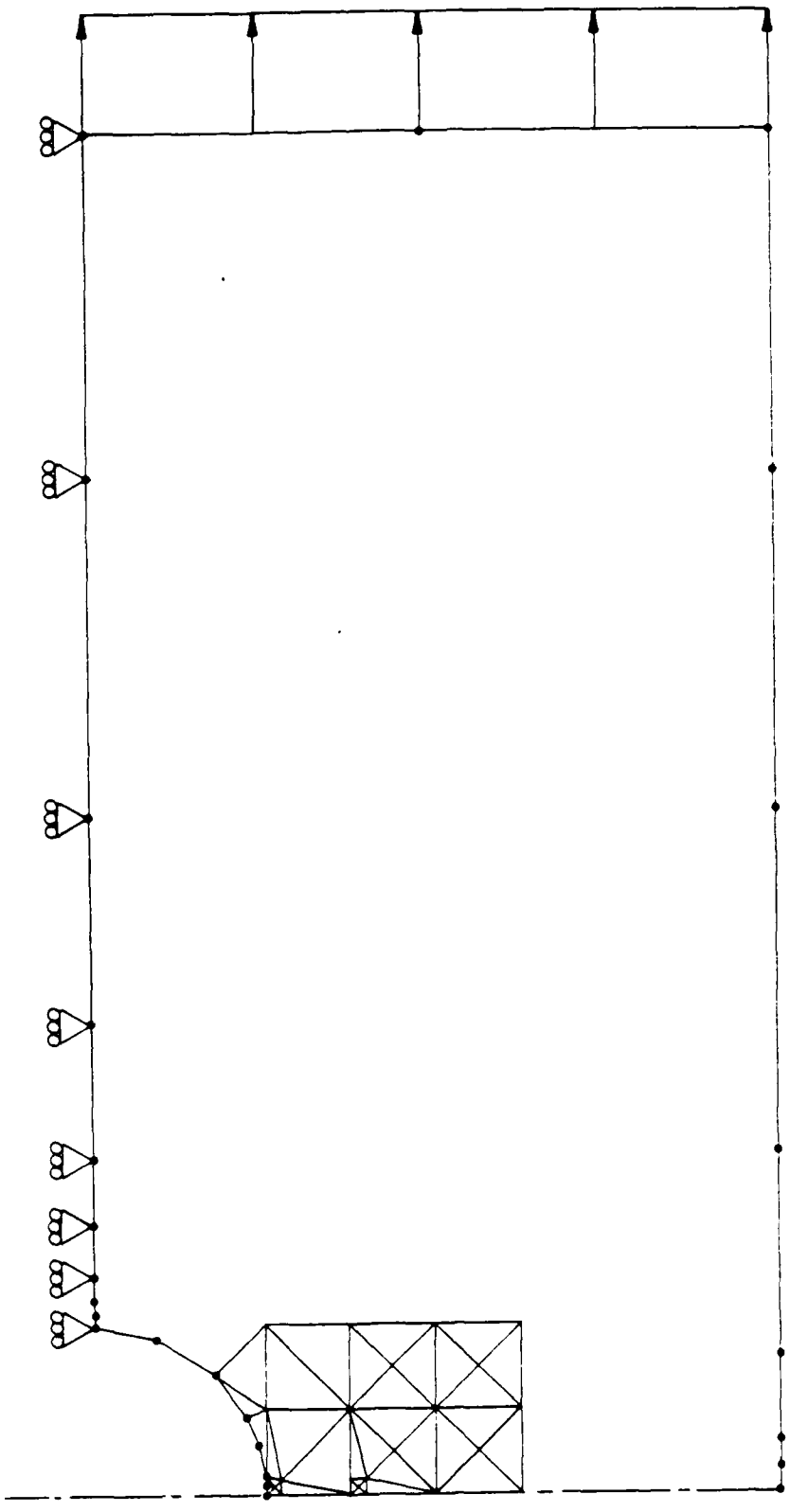

Figure 17. BIE Model of 2:1 Plate with Central Circular Hole (R/W = 0.25)

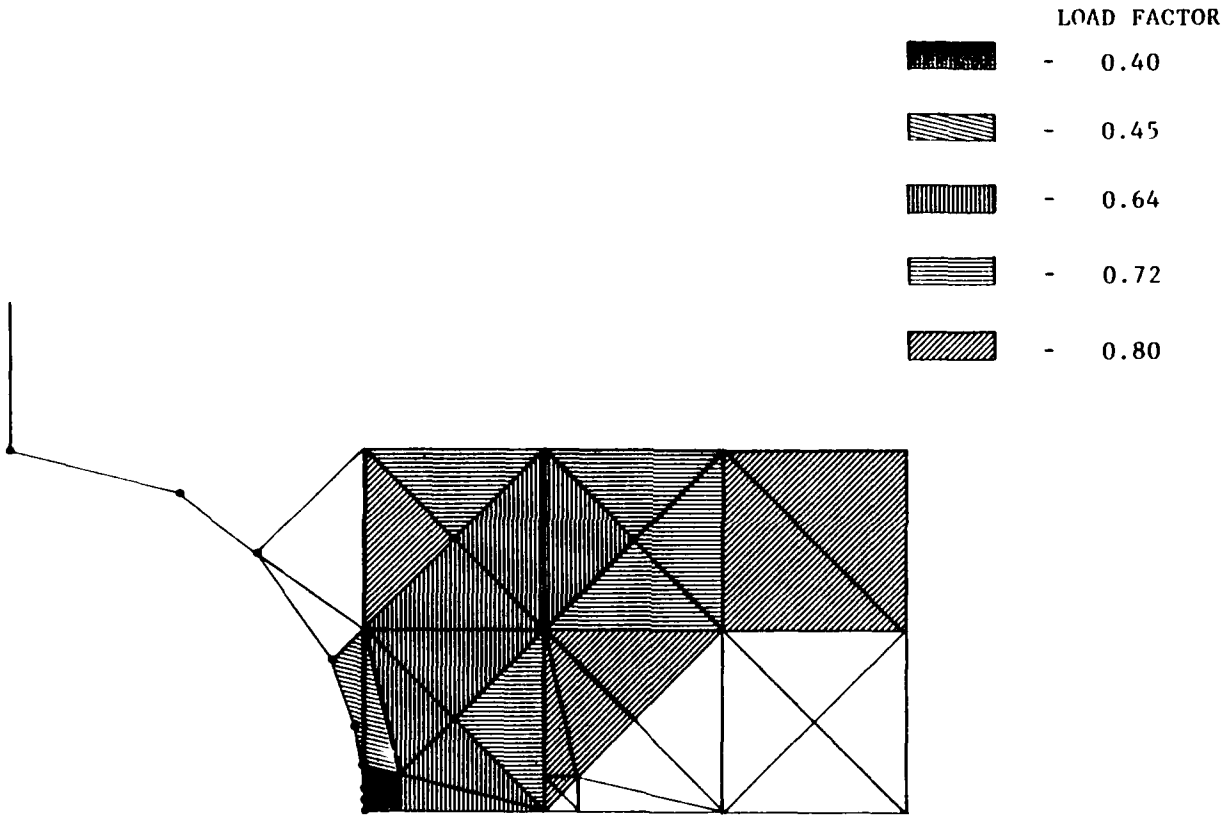

Figure 18. Progressive Generation of Plastic Zone at Hole (Tension Only)

Table 2

Stress Intensity Factor Results $\frac{K_I}{\sigma\sqrt{\pi a}}$

	a/R = 0.05	a/R = 0.5
Elastic		
- Max. load	3.411	2.070
- Zero load	0	0
Plastic (Full Crack Surface Unloading)		
- Max. load	0.843a	1.787[a]
- Zero load	-2.568b	0.283[b]

Note a: Maximum load values (elastically) = Elastic + Zero load values

b: Negative values of KI imply crack closure at positive load

The final example considers the effect of crack tip plasticity on crack closure. The selected plane strain problem, shown in Figure 10, was previously used to validate the BIE/CRX algorithm for elasto-perfectly-plastic crack tip behavior. The plastic strain distribution for this analysis is shown in Figure 11, where a load level of one is net section yield, in plane strain.

The plastic strains in Figure 11 clearly indicate the inverse-crack-tip-distance singular behavior expected from the perfect plasticity solution [15]. As discussed in [3], such a plastic strain singularity does not lead to a convergent volume integral for eq. (4). At the maximum applied load (LF = 0.2075), the elastic stress intensity factor is given by:

$$\frac{K_I}{\sigma\sqrt{\pi a}} = 1.08 \qquad (11)$$

with σ = 11,579 psi and a = 100 inches. Use of the full plastic strains from the perfect-plasticity solution at this load level gives an apparent strength of the elastic singularity (K_I^*)

$$\frac{K_I^*}{K_I} = 1.167 \tag{12}$$

The increase in K_I^* using eq. (4) substantially exceeds the effect of crack tip plasticity on crack driving force that would be predicted using a crack size equal to the physical size plus the plastic zone size. Denoting the plastic zone size by r_p we obtain

$$\frac{r_p}{a} \simeq \frac{\frac{1}{a}\left(\frac{K_I}{\sigma_y}\right)^2}{2\pi} = 0.03 \tag{13}$$

Then the effective crack tip stress intensity factor would be estimated as

$$\frac{K_{eff}}{\sigma\sqrt{\pi a}} = \frac{a + r_p}{a} = 1.015 \tag{14}$$

Thus, we conclude that the singularity contribution to eq. (4) is, in fact, unbounded and the result in (12) is not meaningful.

The unloaded solution to the same crack problem involves reversal of the crack tip plasticity. Figure 19 compares the loaded and unloaded transverse plastic strain (ε_y^P) distributions along the line of maximum equivalent stress. The unloaded plastic strain distribution is much less singular and we compute, at zero load

$$\frac{K_I^*}{\sigma\sqrt{\pi a}} = 0.11 \tag{15}$$

as compared to the value 0.015 estimated in (14). This large result still indicates that the residual strain singularity is still too strong to be neglected in using eq. (4).

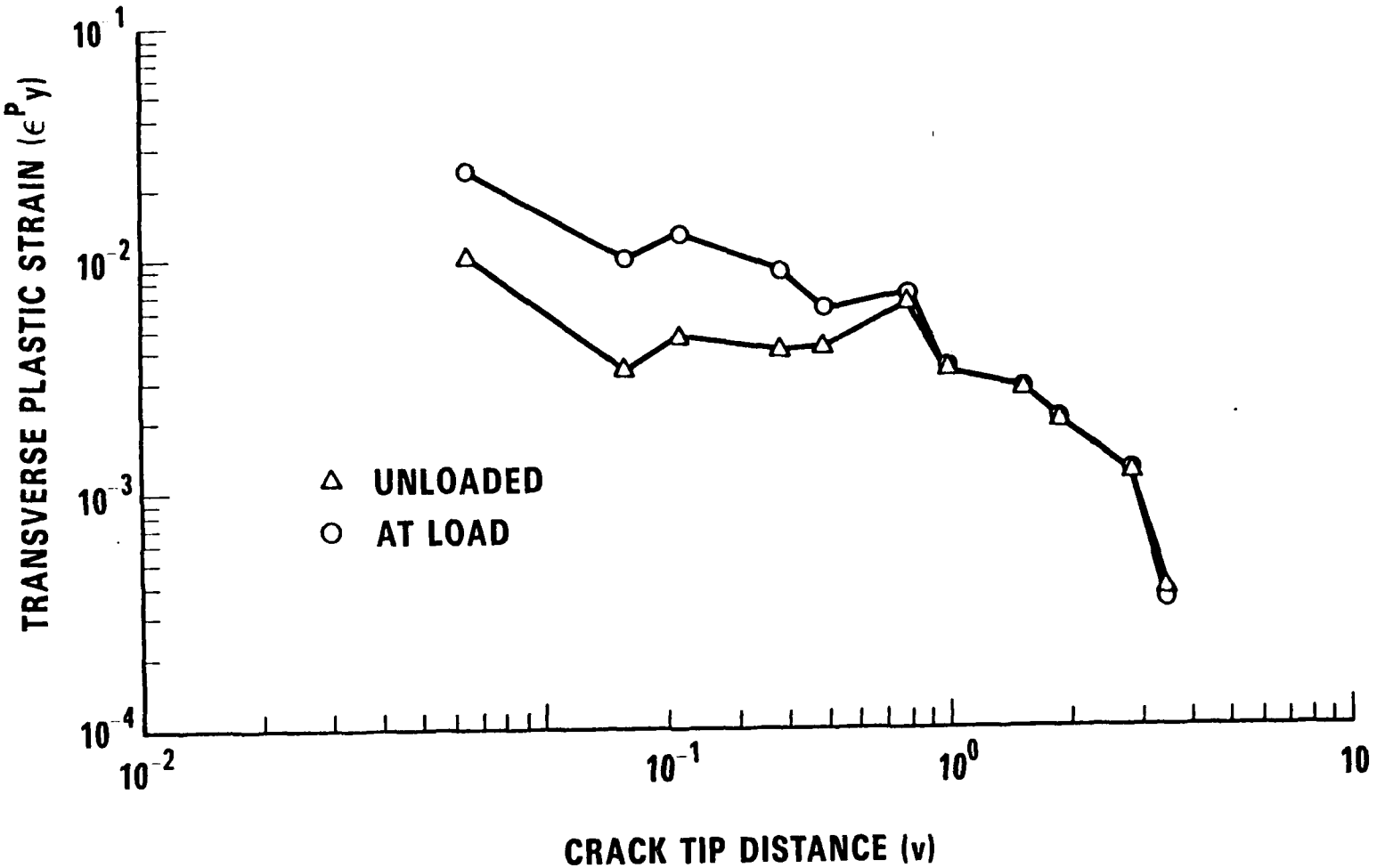

Figure 19. Loaded and Unloaded Transverse Plastic Strain

While the magnitude of (15) is not meaningful, eq. (4) can be used to indicate the relative effect of the residual strains on retardation of crack growth. The approach is the same as used in the notch problem discussed above. That is, the crack is extended elastically into the residual strain field, and K_I^* is recomputed. The result, in Figure 20, is given as $\frac{K_I^*}{K_I}$.

The plot shows almost an instantaneous change of K_I^* at no load to a negative value. This result confirms the expectation of a retardation effect of crack tip plasticity on subsequent cyclic stress intensity factor. The peak effect is at $\frac{r}{r_p} = 0.27$, corresponding roughly to some estimates of the plane strain plastic zone size $\frac{r_p}{3}$; the extent of the retardation zone is $\frac{r}{r_p} = 3$.

Thus, we conclude that the volume integral in eq. (4) is substantially nonconvergent for the crack problem. The correction would be to delete from the plastic strains those due to the singularity alone. It is expected that the remaining plastic strains can be used to compute an effective stress intensity factor which accounts for contained plasticity effects.

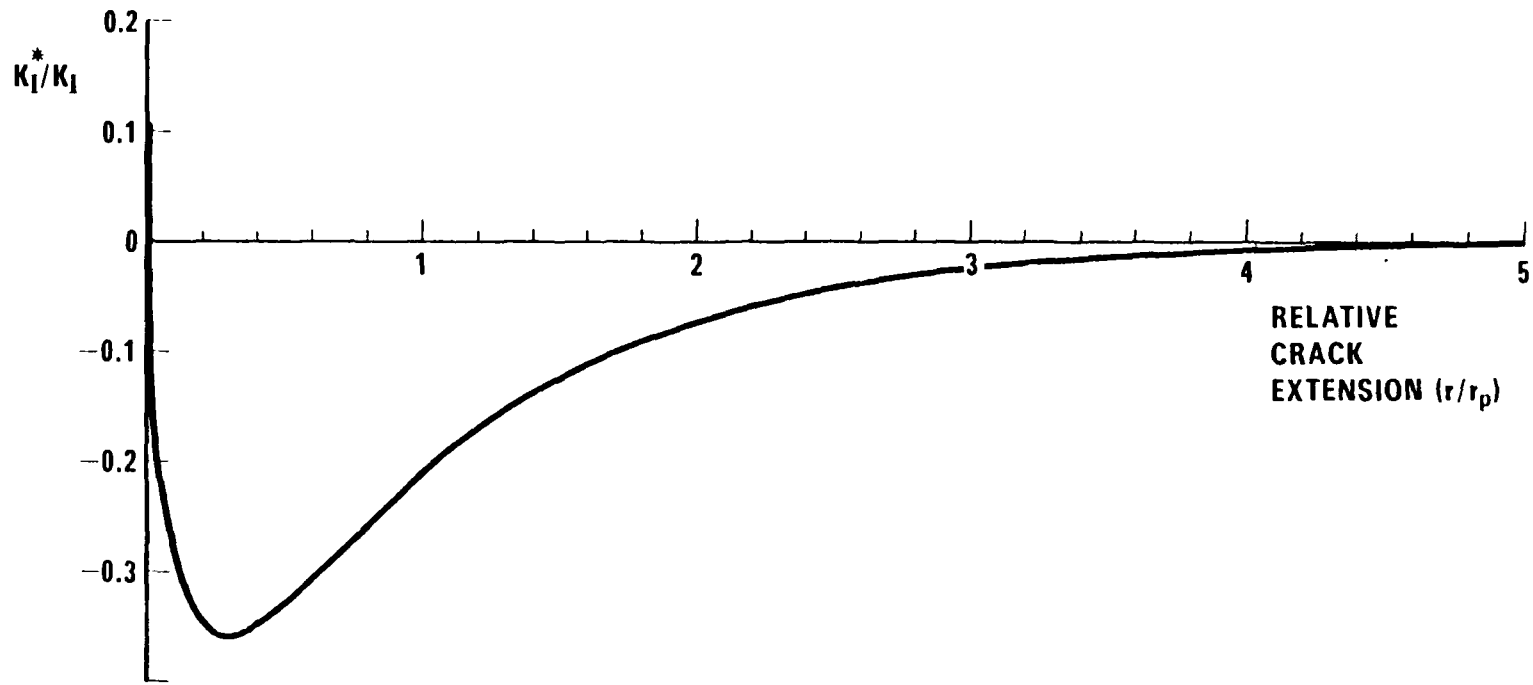

Figure 20. K_I^*/K_I As a Function of Relative Crack Extension

4.0 GENERAL SOLUTION PROCEDURE FOR FRACTURE MECHANICS WEIGHT FUNCTION EVALUATION

4.1 Weight Functions

The weight function method is based on Rice's [16] interpretation of Bueckner's [17] original paper. The weight function for a crack problem is generally taken to be the normalized rate of change of surface displacements with respect to crack size for a reference state of loading. As shown by Rice [16], this weight function acts as a Green's function for the crack problem. That is, the solution to any fracture mechanics problem for the same geometry but different loading conditions can be obtained from the weight function for the reference set of loading conditions. The manner in which this is done will be reviewed in greater detail later in this paper, but the process involves an integration of the uncracked stress field times the weight function to arrive at the crack tip stress intensity factor for those imposed stresses.

The singular advantage of the weight function method is efficiency of computation of the crack tip stress intensity factor for a variety of crack sizes and loading conditions. Crack size effects such as finite width effects on stress intensity factor, or size effects where crack size changes the applied loads (stiffness effects), need to be included in the weight function. The new method reported herein addresses the computational problem of generating weight functions in a direct and efficient manner, while providing for the first time a general method for the mixed-mode problem.

4.2 Numerical Methods for Evaluating Weight Functions

The weight function method discussed herein excludes the related, Green's function method for stress intensity factor evaluation. In the Green's function method, many of which are given in Rooke and Cartwright [18], the

stress intensity factor for the reference problem is given in generalized terms as the response to a point load on the crack surface. The point load solution is then integrated as a weighted integral of the applied tractions.

While the Green's function and weight function methodologies are closely related, the computational approaches for the two methods are distinct. The current paper focuses on the numerical evaluation of surface displacement derivative evaluation to establish the weight function. The approach is based on the boundary element method for two-dimensional fracture mechanics, as first developed by Snyder and Cruse [1], enhanced and corrected by Cruse [2], and most recently used for elastoplastic fracture mechanics modeling by Cruse and Polch [3]. In these reports the general BEM is implemented with augmented boundary integral equation kernels which explicitly include the presence of a stress free crack.

Most numerical methods for the development of weight functions are based on the boundary integral equation, Besuner [19], or finite element methods, Parks [20]. The boundary integral equation solutions (now referred to generally as boundary element methods) have been based upon numerical differentiation of the numerical results. That is, the crack surface displacement numerical solutions are obtained for two slightly different crack lengths. The finite element method was modified by Parks [20] to include in the virtual work principle an explicit derivative with respect to crack size. This permitted the FEM-based approach to be more efficient than numerical differentiation. This approach has been exploited to a great extent by Sha and Yang [21].

A second approach to the numerical problem is that proposed originally by Paris, McMeeking and Tada [22]. In this method, the weight function is computed for the problem of cracked body subject to the elastic singularity

tractions on a small circular path surrounding the crack tip. While most of the results were obtained using the FEM, Cartwright and Rooke [23] used the BEM to obtain very satisfying numerical results. Others, e.g., Grandt [24] and Petroski and Achenbach [25], have developed very efficient means of estimating weight functions for a limited number of specific geometries.

4.3 Formulation

A general purpose numerical evaluation of crack surface weight functions has been developed based on a novel use of a specialized boundary element formulation of the two-dimensional fracture mechanics problem. The following sections will present two-dimensional brief definition of crack surface weight functions, their use, and some of their potential limitations, followed by a review of the new method. The basic references for these discussions are Rice [16] for the weight functions, and Cruse [2] for the boundary element method. The general weight function approach of Bortman and Banks-Sills [26] will be followed.

4.3.1 Crack Surface Weight Function

Consider two solutions for the specified geometry. We will call solution state -(2) as the unknown solution, and solution state -(1) as the reference state. Both solutions consist of stress and strain variables on the interior of the body, and tractions and displacements on the surface. The reciprocal work done by the stresses of solution -(2) on the strains of the reference state is given by*

$$W = \frac{1}{2}\int_V \sigma_{ij}^2 \, \varepsilon_{ij}^1 \, dV = \frac{1}{2}\int_S t_i^2 \, u_i^1 \, dS + \frac{1}{2}\rho \int_V f_i^2 \, u_i^1 \, dV \qquad (16)$$

---

*Superscripts should not be confused with powers in this section.

The boundary integral consists of the tractions t_i^2 and the displacements u_i^1 for the two solutions; f_i^2 is the body force term.

Consider next the virtual extension of the crack for the reciprocal problem. The tractions that are released ahead of the crack in (16) are singular with the usual inverse square-root behavior. The displacement term in (16) is proportional to the square root of crack tip distance. A reciprocal energy release rate can be computed in terms of the mixed-mode stress intensity factors (K_I, K_{II}) for the two solutions. Letting $H = E/(1 - \nu^2)$ for plane strain and $H = E$ for plane stress, we obtain

$$\frac{1}{H}\left(K_I^1 K_I^2 + K_{II}^1 K_{II}^2\right) = \int_{S_t} t_i^2 \frac{\partial u_i^1}{\partial a}\, dS + \int_{S_u} \frac{\partial t_i^2}{\partial a} u_i^1\, dS \qquad (17)$$

The boundary has been divided into that part for specified tractions (S_t) and that for specified displacements (S_u). The body force term in (17) has been dropped only for simplicity at this point. Since state -(2) is general, we can compute equation (17) for another general (and independent) solution. The reciprocal strain energy release rate in (17) then gives

$$\frac{1}{H}\left(K_I^1 K_I^3 + K_{II}^1 K_{II}^3\right) = \int_{S_t} t_i^3 \frac{\partial u_i^1}{\partial a}\, dS + \int_{S_u} \frac{\partial t_i^2}{\partial a} u_i^1\, dS \qquad (18)$$

Combining equations (17) and (18) we can solve for the stress intensity factors for the arbitrary problems in terms of the solution of the reference problem

$$K_I^1 = \frac{H}{2(K)^2} \left[K_{II}^3 \int_{S_t} t_i^2 \frac{\partial u_i^1}{\partial a} dS + \int_{S_u} \frac{\partial t_i^2}{\partial a} u_i^1 dS \right. \tag{19a}$$

$$\left. - K_{II}^2 \int_{S_t} t_i^3 \frac{\partial u_i^1}{\partial a} dS + \int_{S_u} \frac{\partial t_i^3}{\partial a} u_i^1 dS \right]$$

$$K_{II}^1 = \frac{H}{2(K)^2} \left[K_I^2 \int_{S_t} t_i^3 \frac{\partial u_i^1}{\partial a} dS + \int_{S_u} \frac{\partial t_i^3}{\partial a} u_i^1 dS \right. \tag{19b}$$

$$\left. - K_I^2 \int_{S_t} t_i^2 \frac{\partial u_i^1}{\partial a} dS + \int_{S_u} \frac{\partial t_i^2}{\partial a} u_i^1 dS \right]$$

where $$(K)^2 = K_I^2 K_{II}^3 - K_{II}^2 K_I^3 \neq 0 \tag{20}$$

In the case of symmetric loading, equation (20) reduces to

$$K_I^2 = \frac{H}{2K_I^1} \left[\int_{S_t} t_i^2 \frac{\partial u_i^1}{\partial a} dS + \int_{S_u} \frac{\partial t_i^2}{\partial a} u_i^1 dS \right] \tag{21}$$

This is the same form as developed by Rice [16] except for the introduction of mixed boundary conditions. The solution approach using weight functions is normally given for $S_u = 0$ such that

$$K_I^2 = \frac{H}{2K_I^1} \int_S t_i^2 \frac{\partial u_i^1}{\partial a} dS = \int_S t_i^2 h_i^1 dS \tag{22}$$

where $h_i^1(S)$ is the weight function. For the mixed boundary value problem, no simple weight function can be written down and the full form of equation (21) has to be used.

Thus, for the general weight function method, one needs an efficient means for solving the reference geometry fracture mechanics problem, subject to any fixed displacement or compliant boundary conditions, to obtain the rate of change in boundary displacements and tractions, and the crack tip stress intensity factors. The fracture mechanics BEM provides the most direct and efficient means for providing this data in the appropriate manner.

4.3.2 Boundary Integral Equation Formulation

The boundary element formulation of the two-dimensional fracture mechanics problem is restated for completeness in a shortened notation

$$\mathbf{u}/2 + \int_S \mathbf{T}^* \mathbf{u}\, dS = \int_S \mathbf{U}^* \mathbf{t}\, dS \qquad (23)$$

where the physical variables are the boundary displacement and traction vectors, $\mathbf{u}$, $\mathbf{t}$. The kernel functions $\mathbf{U}$, $\mathbf{T}$ in (23) are the displacement and traction (on S) solutions to the elasticity problem for the infinite plane subject to a point force loading; these functions are known as fundamental solutions in the BEM. The asterisk on each of the fundamental solutions denotes further that they represent the solution for the point load in an infinite plane, containing a single, traction free crack of length 2a. The surface S in (24) does not include the crack surface, as these boundary conditions are automatically satisfied by the special Green's function or fundamental solution used in this formulation.

The weight function method requires the solution in terms of the rate of change of the boundary conditions, as a function of crack length. Differentiation of (23) with respect to crack length is completely straightforward, due to the explicit dependence on crack length of the kernels of the integral operators. Thus, we obtain the following boundary identity

$$\frac{\partial u}{\partial a} + \int_{S_t} T^* \frac{\partial u}{\partial a}\, dS - \int_{S_u} U^* \frac{\partial t}{\partial a}\, dS = - \int_{S} \frac{\partial T^*}{\partial a}\, u\, dS + \int_{S} \frac{\partial U^*}{\partial a}\, t\, dS \qquad (24)$$

The boundary has been denoted as $S = S_u + S_t$ to denote the notions of both displacement and traction boundary conditions on portions of the surface. In general, the mixed boundary conditions involve somewhat more complexity than is denoted by this notation, but the terms in (24) convey the essential notion of the algorithm.

Letting the vector **x** correspond to the unknown boundary conditions (both traction and displacement components), and **y** the known boundary conditions, a symbolic form of (24) may be written

$$[\mathbf{A}] \begin{Bmatrix} \partial u/\partial a \\ \partial t/\partial a \end{Bmatrix} = [\mathbf{A}]\{\mathbf{x}\} = [dB/da]\{\mathbf{y}\} \qquad (25)$$

Equation (25) is obtained from (24) by the imposition of a boundary interpolation system. In the current application, the boundary data is assumed to vary in a piecewise linear fashion, with **x**, **y** representing nodal variables.

Equation (25) is very similar to the discrete form of the BIE (23) which is solved to obtain the unknown boundary conditions for the reference problem. Specifically, **A** is identically the same as for the boundary value problem. The right-hand-side of (25) is made up of the derivative of the **B** terms with respect to the crack length, and **y** is the totality of boundary data from the solution of the reference problem, equation (23).

Thus, the algorithm for the solution of (25) consists of

1. setting up the discrete form of (23) to obtain **A**,
2. storing **A** for later use,
3. solving for the unknown boundary data,

4. computing the elements of [dB/da],

5. solving (25) using the entirety of the boundary conditions

The solution to (25) consists of the change in all non-specified boundary conditions, except along the crack surface. This is so because the special Green's function used for the fracture mechanics solution automatically satisfies the crack surface conditions, and the crack surface is eliminated from (23). The complete solution therefore requires an additional step before the full weight function can be defined.

The BEM is based on the so-called Somigliana identity for the interior solution variable, which in this case is the displacement variable. The derivative of the interior displacements corresponding to the boundary solution to (23) is given by

$$\partial u/\partial a = - \int_S T^* \frac{\partial u}{\partial a} \, dS + \int_S U^* \frac{\partial t}{\partial a} \, dS - \int_S \frac{\partial T^*}{\partial a} u \, dS + \int_S \frac{\partial U^*}{\partial a} t \, dS \qquad (26)$$

Equation (26) is equally true for interior points or crack surface points, although care must be exercised in the evaluation of the kernel functions for crack surface points. The numerical solution of (26) completes the weight function description, in a formal way. That is, by specifying a suitable number of crack surface locations, the analyst is given a complete description of the rate of boundary condition change with respect to crack length, as needed in equation (21). However, the term from (26) for the point at the crack tip is singular and requires special treatment, as discussed in the next section.

4.3.3 Crack Tip Stress Intensity Factor

One of the very important features of the fracture mechanics BIE solution is direct access to a very accurate and generic algorithm for evaluating the crack tip stress intensity factors for mixed mode response. This

algorithm has been previously discussed and requires only that the following integrals be evaluated for some path in the cracked body

$$K_{I,II} = - \int_S R_{I,II} \mathbf{u} \, dS + \int_S L_{I,II} \mathbf{t} \, dS \tag{27}$$

The complete traction and displacement solution needs to be specified on some path, and the original surface (excluding the crack surface) is usually selected. However, as discussed in Cruse [27], the algorithm is independent of path and has successfully been used as a post-processing algorithm even for finite element models.

The weight function algorithm also involves the direct computation of a crack tip singularity. Taking the free term in (26) to be evaluated near the crack tip, it has been found that the kernels contain an explicit, square-root singularity. As in the development of (27) we take the integral identity (26) for points near the crack tips (either end of the crack), multiply by the square root of crack tip distance and proceed, in the limit, to the crack tip. A non-singular form of (26) is then obtained

$$\lim_{r \to 0} \sqrt{r} \frac{\partial \mathbf{u}}{\partial a} = S_{I,II} = - \int_S \mathbf{T}\mathbf{u} \, dS + \int_S \mathbf{U}\mathbf{t} \, dS \tag{28}$$

where

$$\mathbf{T} = \lim_{r \to 0} \sqrt{r} \frac{\partial \mathbf{T}^*}{\partial a} \quad , \quad \mathbf{U} = \lim_{r \to 0} \sqrt{r} \frac{\partial \mathbf{U}^*}{\partial a} \tag{28a}$$

These terms are directly related to the stress intensity factors found in (27), but are derived from a completely independent basis. Thus, they provide a validation of equation (25) by comparison to the results from equation (27). Having the explicit, limiting singularity strength provides the analyst with a complete description of the weight function for the reference problem.

4.4 Applications

The applications given in this paper are limited to validation examples for the computational algorithm that has been developed. No effort to compute stress intensity factors from the BEM-developed weight functions will be given, as these are covered adequately in the references given. The following sections will present a brief description of the computational implementation of the BEM-weight function algorithm, two numerical examples of interest, and some conclusions based on the work done to date.

4.4.1 Programming

The BIE (23) is first formulated, making direct use of the defined boundary conditions to assemble the matrix for the unknown boundary data. The right hand side vector is assembled from the product of the kernel functions and the specified boundary data. The coefficient matrix is stored on tape for later recall, and the system of equations is solved by reduction. The full set of boundary data is then completed and the coefficient matrix recalled. The new right hand side vector is formed from the matrices resulting from differentiation of the standard kernels, with respect to crack length, times the full set of boundary data for the reference problem. Re-reduction of the same matrix then results in the set of boundary data corresponding to rates of change with respect to crack length. Mixed boundary conditions and mixed-mode cracking problems are handled directly.

The next step is to compute the crack tip terms at one or both of the crack tips and the rate of change of crack surface displacements with respect to crack length. The same matrices as used for the boundary terms above are computed for the points located on the crack surface. These points are input as percentages of crack length, and are taken to be on the top surface of the crack for symmetric problems.

4.4.2 Numerical Examples

Two example reference problem calculations are presented which illustrate the essential numerical capabilities of the weight function calculation procedure. The first is more in the way of a validation example, as the problem considered is a simple square plate with a central crack, Figure 21. The plate is loaded in simple tension transverse to the crack as shown; this loading results in Mode I response of the crack. The crack sizes range from a/W = 0.01 to 0.5.

The smallest crack size is essentially equal to the infinite plate problem. The computer code calculated stress intensity factors for each case; for the short crack case the accuracy to the infinite plate result was to five significant figures. Figure 22 plots the normalized crack opening displacement derivative results for the four cases. It is seen that in all cases the resulting distribution is quite smooth over most of the crack; the finite width effect is seen for the cases of a/w > 0.1. The normalized crack tip singular behavior is also seen in Figure 22 to be essentially identical for each of the cases. The stress intensity factor computed for the crack opening displacements, using equation (28), was essentially identical to the previously exploited algorithm based on internal stresses, equation (27).

Figure 23 shows the BEM mesh for the second reference problem considered in this study. The problem is a plate with a central hole and an edge crack from the hole. The mesh was established in a manner that represented mixed boundary conditions, as the left-hand side is taken as a plane of simulated symmetry.

The crack is taken to be located at the horizontal symmetry line, extending from the edge of the crack. It is to be re-emphasized that the BEM algorithm being used does not model the surface of the crack, as this surface

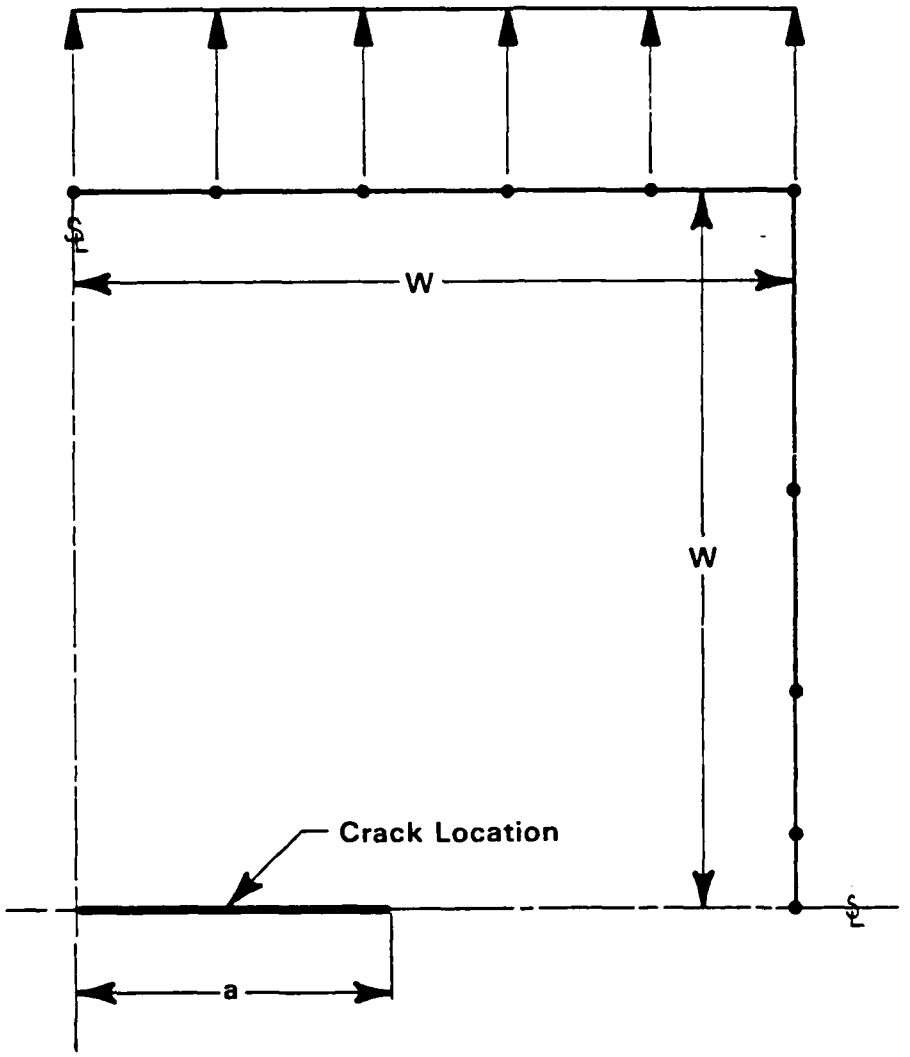

Figure 21. Validation Example: Square Plate with Central Crack

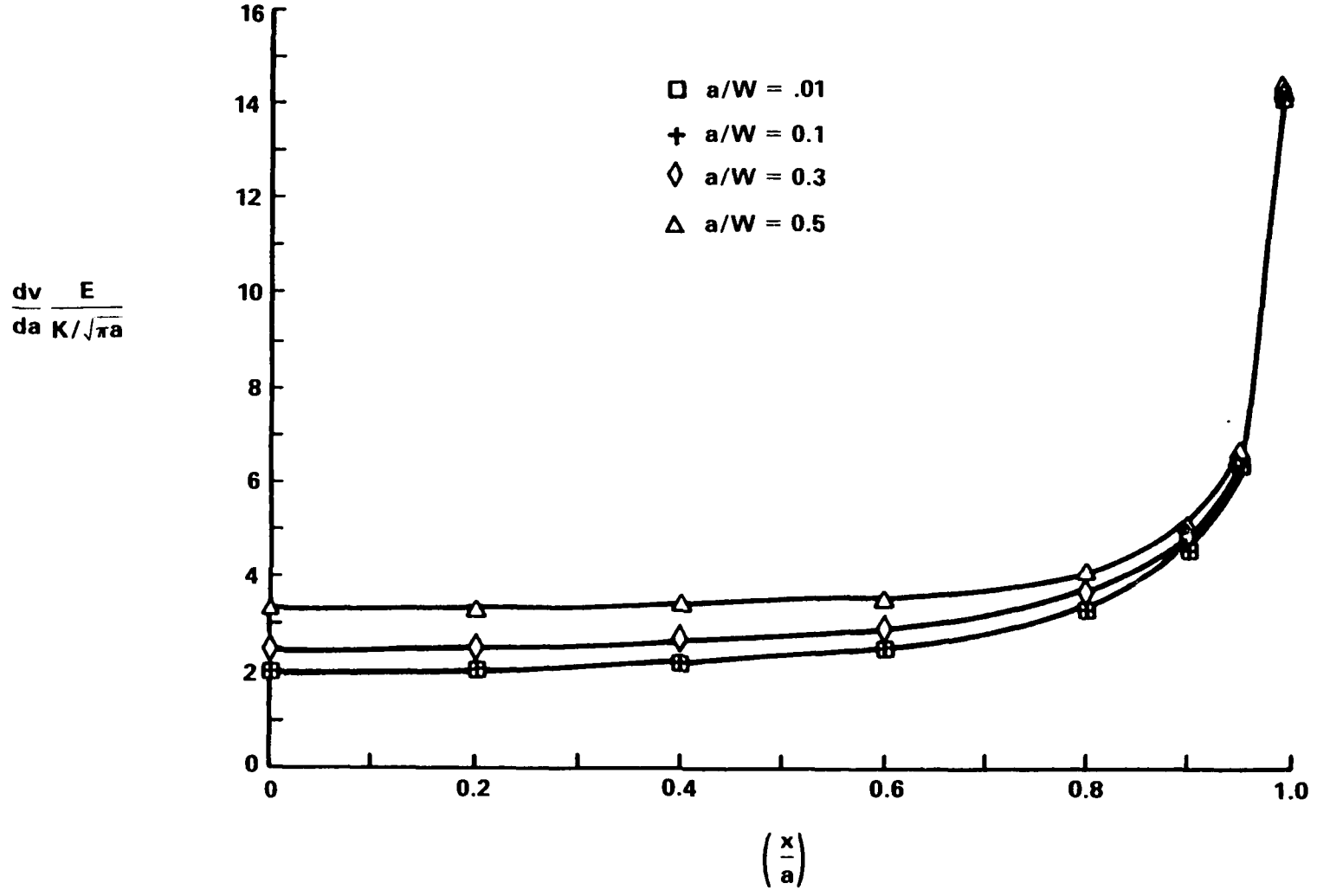

Figure 22. Weight Function Data: Tension Plate with Center Crack

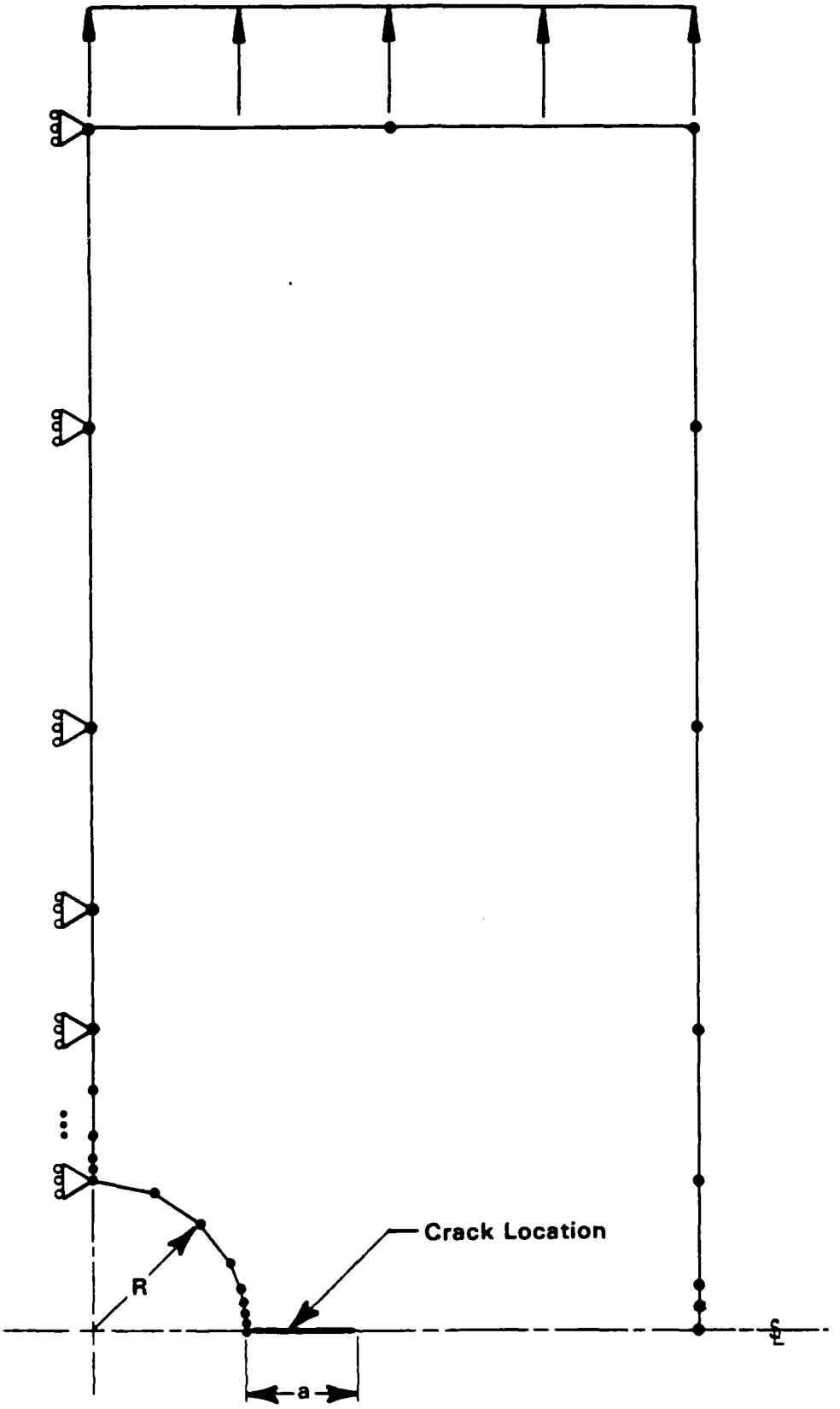

Figure 23. BEM Mesh for Plate with Central Hole and Edge Crack

is explicitly and exactly accounted for in the formulation of the integral equations. The plate is taken to be sixteen units long, with a width of eight units and a hole radius of two units.

Figure 24 plots the computed stress intensity factors for five crack sizes (a/R = 1.5, 1, 0.5, 0.25, and 0.05). The stress concentration factor for the hole is computed to be 3.59 versus the value of 3.54 from Peterson [15]. The stress intensity factor for an infinitesimally short edge crack at the hole is then given by

$$K_I = 1.12\ K_T\ \sigma\ \sqrt{\pi a} \tag{29}$$

The value of normalized stress intensity factor in Figure 24 for a/R = 0, therefore, is 3.98. The stress intensity factor is seen to decrease with increasing crack size for short crack lengths due to the effect of the stress gradient. For longer crack lengths, the values are seen to begin to rise, as would be expected due to finite width effect. The second curve in Figure 24 simply normalizes the stress intensity factor such that the value at a/R = 0 is zero.

Figures 25 and 26 present the numerical results for the normalized weight function for the Mode I reference problem. The results in Figure 25 are essentially of the same shape as in Figure 22, although the zero intercept is elevated due to the free edge effect. Also the order of the curves is affected by a/R. Figure 26 normalizes these results by the numerical results for the center cracked panel (a/W = 0). The case for a/R = 0.05 clearly shows the influence of the free edge effort for short cracks while the others begin to look more like the results for a center cracked panel of crack length equal

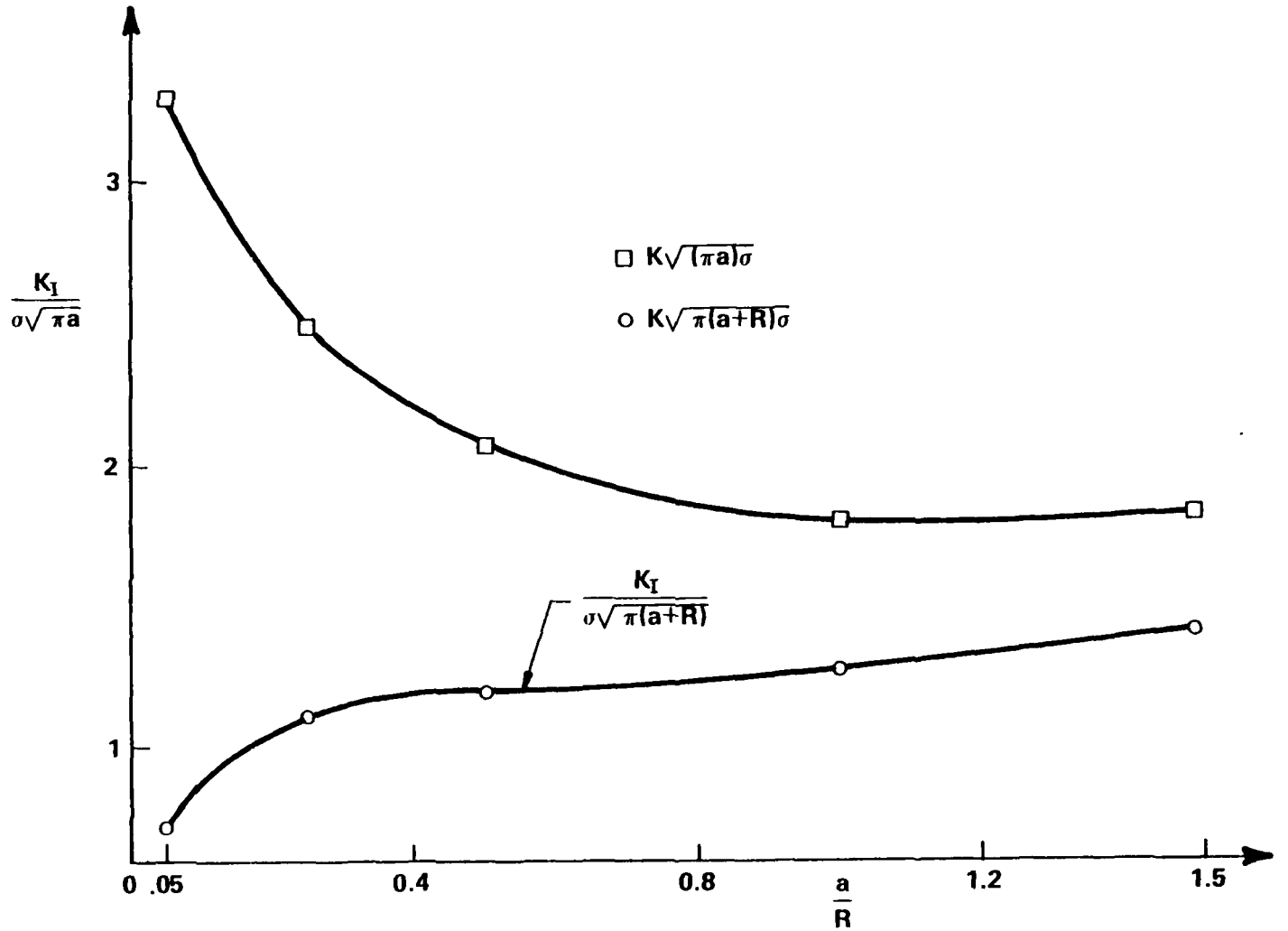

Figure 24. Stress Intensity Factions: Tension Plate with Hole

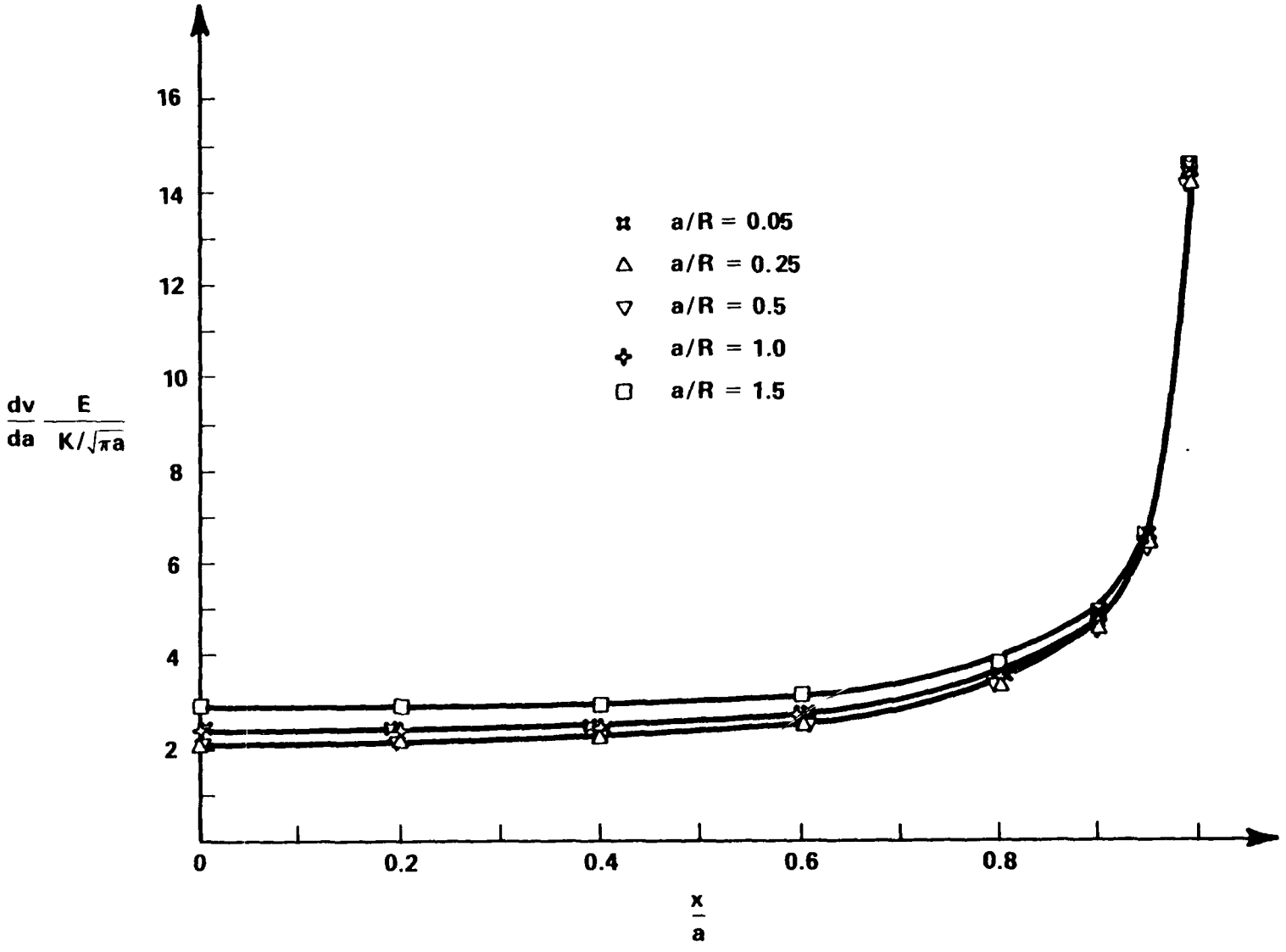

Figure 25. Weight Function Data: Tension Plate with Hole

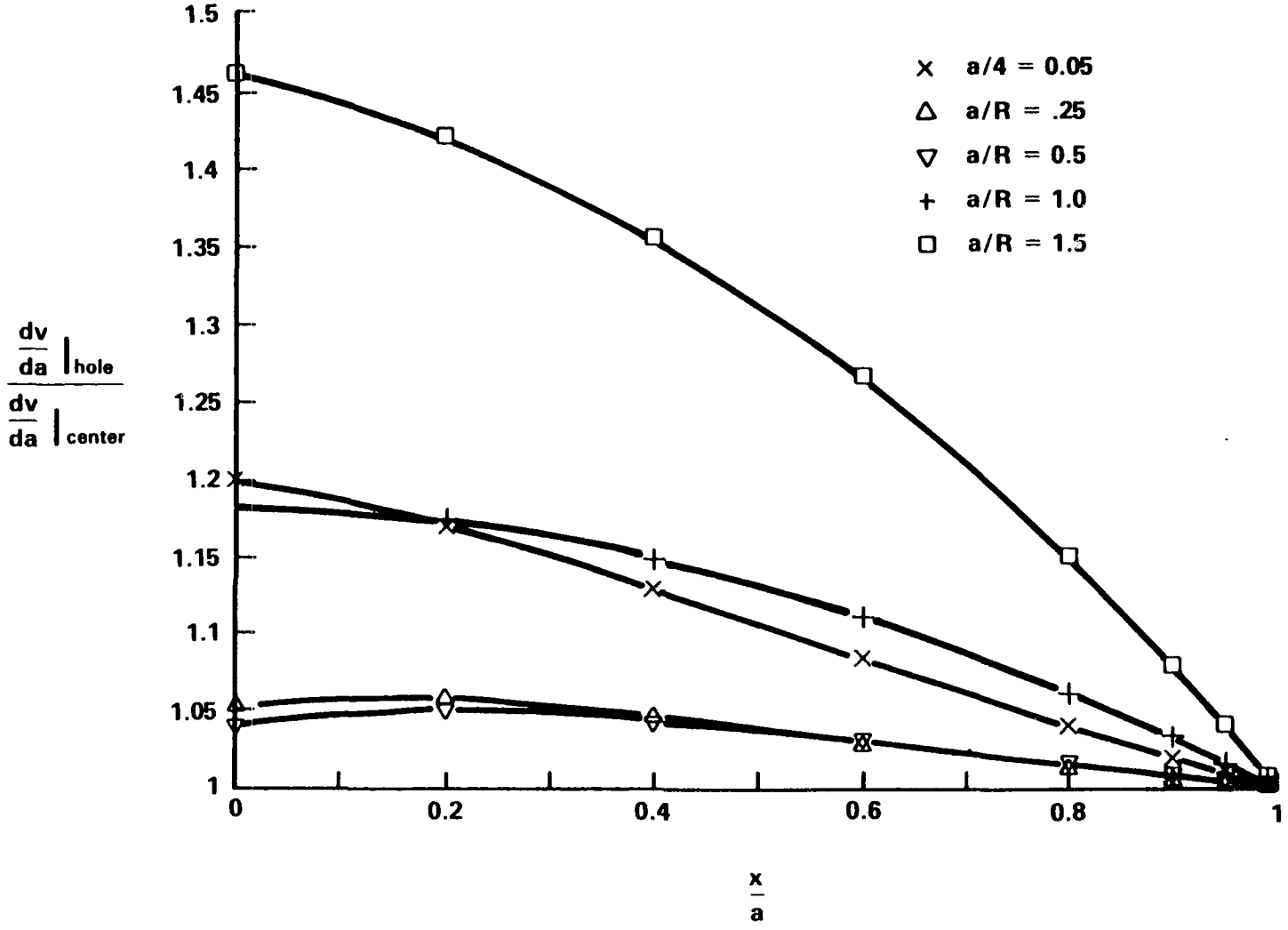

Figure 26. Weight Function Data: Tension Plate with Hole Center Crack

to (a + R). The singular behavior of all of these solutions is essentially identical to the center cracked results, in the normalized presentations of Figures 22 and 26.

5.0 BURIED CRACK ANALYSIS WITH AN ADVANCED TRACTION BIE ALGORITHM

5.1 Introduction

The algorithm for analysis of buried cracks of arbitrary shape, presented in this section, is a part of a bigger code. The ultimate goal of the principal code is a solution of an arbitrary surface crack problem. The alternating boundary traction method (Nishioka and Atluri [28]) is used to this end. Both the literature and our experience show the efficiency and good convergence properties of the alternating method. The accuracy of the solution of a buried crack problem, being the main part of the alternating method algorithm, plays the most important role in the accuracy of the overall results.

The problem of a buried crack with arbitrary geometry has not been solved satisfactorily. Nishioka and Atluri [28] used a solution based on Jacobi potential functions for the elliptical planar geometry and polynomial loading. Weaver [29] used a dislocation model to solve the problem for the case of the rectangular crack. Using the same dislocation method, Bui [30] presented a solution for an arbitrary geometry, but with poor accuracy. The accuracy of Bui's method has been improved by Putot [31], albeit with certain artifices. The current work, reported herein, removes these limitations and deficiencies by a successful combination of quite well known numerical techniques.

5.2 Mathematical Statement of the Problem

The problem of a loaded crack in an infinite three-dimensional body can be mathematically described by a set of integral equations of the first kind for relative crack opening displacements v_i^* in terms of crack surface tractions σ_{i3}.

$$\sigma_{33}(P) = \frac{\mu}{4\pi(1-\nu)} \int_{\langle\Gamma\rangle} \frac{r_{,\alpha} v_{3,\alpha}}{r^2} dS \quad (\alpha,\beta=1,2)$$

$$\sigma_{13}(P) = \frac{\mu}{4\pi(1-\nu)} \int_{\langle\Gamma\rangle} \left[\frac{v_{\beta,\beta} r_{,1}}{r^2} + (1-\nu) \frac{(v_{1,2}-v_{2,1}) r_{,2}}{r^2}\right] dS \qquad (30)$$

$$\sigma_{23}(P) = \frac{\mu}{4\pi(1-\nu)} \int_{\langle\Gamma\rangle} \left[\frac{v_{\beta,\beta} r_{,2}}{r^2} + (1-\nu) \frac{(v_{2,1}-v_{1,2}) r_{,1}}{r^2}\right] dS$$

where

$$r^2(P,Q) = \sum_{i=1}^{3} (x_i(P) - x_i(Q))^2 \; ; \; v_{i,\alpha} = v_{i,\alpha}(Q)$$

$\langle\Gamma\rangle$ denotes integration over Γ in the Cauchy Principal Value sense.

This well-known set of equations (Weaver [29]), Bui [30], Cruse [27])is herein called the Traction Boundary Integral Equation. The Greek subscripts apply to the in-plane directions defined by the normal direction, X_3. This set of equations is derived from the Somigliana identity for the internal stresses in a body with the crack (Cruse [27]). An important feature of this representation of the physical problem is that it decreases the dimensionality of the problem from three to two, the equations extending only over the two-dimensional crack surface.

---

* $v_i = u_i$ (upper surface) - u_i (lower surface) = u_i

An important aspect of the set of equations (30) is the presence of principal value integrals. The evaluation of principal value integrals usually involves special treatment of exclusion circles for singularity. Proper handling of this practical problem requires continuity of displacement gradients (crack surface strains) between the elements. If the continuity condition is not satisfied, certain artifices have to be used to contain the error (Putot [31]).

5.3 Current Numerical Method

In the current numerical method, we use a finite element interpolation scheme for the unknown displacement discontinuities at the crack surface, and their derivatives. In the following, we will use the term "displacements" for "displacement discontinuities" for brevity. The finite element interpolations produce undesirable discontinuities of displacement derivatives at boundaries of the elements unless higher order derivatives are used as nodal quantities.

A special interpolation procedure is used to remedy the problem. We model the displacement field on the crack surface using quadratic 8-noded isoparametric elements, and the displacement gradient field using linear, 4-noded isoparametric elements. The relationship between these two interpolations is established by the following schemes.

The interpolation of the displacement discontinuity field on a crack is given by the relation

$$v_i(P) = \Delta u_i(P) = N^k(P)\Delta u_i{}^k = N^k(P)v_i^k \qquad (31)$$

where

$k = 1,n$

P = point on the crack surface

n = number of nodes of 8-noded element meshes

We will call the displacement interpolation mesh using the 8-noded element the N-mesh in the following discussion. Differentiation of v_i with respect to the global variable x_α will provide the in-plane displacement gradient field

$$v_{i,\alpha}(P) = \frac{\partial v_i}{\partial x_\alpha}(P) = \frac{\partial N^k}{\partial x_\alpha}(P) \quad v_i{}^k \qquad (\alpha=1,2) \tag{32}$$

This field will be, in general, discontinuous at the element boundaries (as the stresses and strains are in standard finite elements).

To find a continuous displacement gradient field corresponding to the original displacement field, we will create a new mesh of linear 4-noded isoparametric elements, referred to as the M-mesh. This new mesh will interpolate displacement gradients on crack surface according to the following

$$v_{i,\alpha}(P) = M^j(P) v_{i,\alpha}{}^j \tag{33}$$

where

$j = 1,m$

m = number of nodes of 4-noded element mesh

The nodes of the M-mesh will coincide with those of the N-mesh and with the centers of 8-noded elements in a manner shown in Figure 27.

We will find the nodal values of displacement gradients by minimizing the difference between the two interpolations, (32) and (33). The difference between the interpolations on the whole crack surface (indices k,j running through all nodes of the crack model) can be written in shorter form as $E_{i\alpha}$ where

$$E_{i\alpha}(P) = \frac{\partial N^k}{\partial x_\alpha}(P) v_i{}^k - M^j(P) v_{i,\alpha}{}^j \qquad \begin{array}{l} k = 1,n \\ j = 1,m \\ i = 1,3 \\ \alpha = 1,2 \end{array} \tag{34}$$

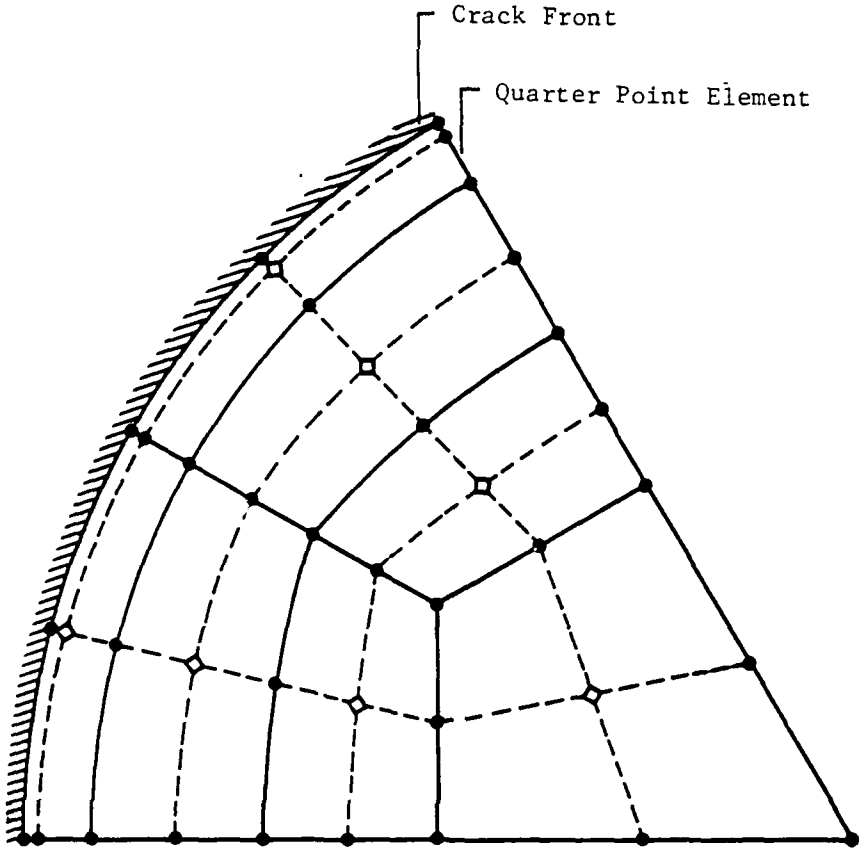

● - Node of the N-mesh

◇ - Extra node of the M-mesh

Figure 27. Interpolation Meshes on Crack Surface

Using the Galerkin weighted residual process, with the same weighting functions as the displacement gradient interpolation shape functions, we obtain the following

$$\int_S E \cdot M^r dS = 0 \qquad r = 1,m \tag{35}$$

Substitution of equation (5) results in

$$\int_S \frac{\partial N^k}{\partial x_\alpha} v_i{}^k M^r dS = \int_S M^j v_{i,\alpha}{}^j M^r dS \qquad r=1,m \tag{35a}$$

or

$$\int_S M^j M^r dS \cdot v_{i,\alpha}{}^j = \int_S \frac{\partial N^k}{\partial x_\alpha} M^r dS \cdot v_i{}^k \qquad r=1,m \tag{35b}$$

The matrix representation of equation (35b) takes on the following form

$$[MM]\{v_{i,\alpha}\} = [NM]\{v_i\} \tag{36}$$

where

$[MM]$ = square matrix of dimensions 6m x 6m with $MM_{jr} = \int_S M^j M^r dS$

$[NM]$ = rectangular matrix of dimension 6m x 3n with $NM_{kr\alpha} = \int_S \frac{\partial N^k}{\partial X_\alpha} M^r dS$

$\{v_{i,\alpha}\}$ = column vector of nodal displacement gradients (dimension 6m x 1)

$\{v_i\}$ = column vector of nodal displacements (dimension 3n x 1)

Matrix MM has the same structure as the finite element consistent mass matrix; clearly, MM is positive definite. Nodal values of the displacement gradients are then calculated by

$$\{v_{i,\alpha}\} = [MM^{-1}]\ [NM]\ \{v_i\} \tag{37}$$

This process very closely resembles global stress smoothing used sometimes in the finite element method, Hinton and Campbell [32]. Since MM is positive definite and has a strongly dominant diagonal, its inversion does not present any problems. In short, the global relationship between nodal displacement gradients and displacements can be written as

$$\{v_{i,\alpha}\} = [MNM]\ \{v_i\} \tag{38}$$

$$\text{where}\quad [MNM]_{6m\ x\ 3n} = [MM^{-1}]\ [NM]$$

The numerical solution of the traction BIE, equation (30), uses the collocation method to form the equivalent system of algebraic equations for the unknowns. Since the displacement mesh contains n nodes with three unknown components of displacements each, we take these nodal locations as collocation points.

The continuous representation of displacement gradients given by (38) allows for very easy and natural treatment of the principal value integrals appearing in (30). It can be easily proven that the basic component of all integrals in (30) vanishes as the radius of an exclusion circle Γ_ε around the source point P goes down to zero, viz.

$$I_{i\alpha\beta}(P) = \lim_{\varepsilon \to 0} \int_{\Gamma_\varepsilon} V_{i,\alpha}(Q)\, \frac{r,_\beta(P,Q)}{r^2(P,Q)}\, dS(Q) = 0 \qquad \begin{matrix} i = 1,3 \\ \alpha = 1,2 \\ \beta = 1,2 \end{matrix} \tag{39}$$

Discretization of the set of equations (30) with the interpolation scheme (33) at n collocation points gives the following system of equations

$$[VV] \cdot \{v_{i,\alpha}\} = \{\sigma_{13}\} \qquad \begin{matrix} i = 1,3 \\ \alpha = 1,2 \\ 1 = 1,3 \end{matrix} \tag{40}$$

where

$[VV]$ - 3n x 6m array of coefficients

$\{v_{i,\alpha}\}$ - 6m x 1 column vector of unknown displacement gradients

$\{\sigma_{13}\}$ - 3n x 1 column vector of known surface stresses (tractions)

This underdetermined system cannot be solved directly for the displacement gradients. To reduce the number of unknowns, we use relation (38), thus changing the unknowns to displacements. We obtain

$$[VV] \cdot [MNM] \cdot \{v_i\} = \{\sigma_{13}\} \tag{41}$$

or

$$[VK] \cdot \{v_i\} = \{\sigma_{13}\} \tag{42}$$

where

$$[VK]_{3nx3n} = [VV][MNM]$$

is the final array of coefficients. System (42) has 3n displacement components as unknowns and 3n equations formulated at n nodes of the displacement mesh. It can be solved by any convenient numerical technique after application of displacement boundary conditions (43) at the contour of crack surface

$$v_i^k = 0 \qquad (i = 1,3; k = \text{node numbers}) \tag{43}$$

The structure of the system of equation (42) shows that (for the current formulation for plane cracks) the problem may be separated into two separate systems of equations. Crack opening displacements are not coupled through the equations with in-plane displacements; thus the system effectively splits into two separate systems of equations

$$[VK_{xy}] \cdot \{v_i\} = \{\sigma_{13}\} \qquad \begin{matrix} i = 1,2 \\ l = 1,2 \end{matrix} \tag{43a}$$

$$[VK_z] \cdot \{v_3\} = \{\sigma_{33}\} \tag{43b}$$

This property allows for greater efficiency of numerical solution-systems of equations for separate sub-problems are smaller than the full system. The decoupling of the system is used in the computer implementation of the method. After solution of system (42) the displacement gradients at m nodes of the linear element mesh can be obtained using equation (38).

Stresses at any location of the infinite body due to crack loading (except for the crack surface itself) can then be obtained using formula (44)

$$\sigma_{i\alpha}(p) = - \int_\Gamma S_{li\alpha}(p,Q) v_l(Q) dS(Q) \tag{44}$$

The kernel S_{lia} is given in Cruse [33]. To calculate integral (44), we use the displacement interpolation (31) on the N-mesh. Integral (44) presents no particular problems, since it is a proper one. Higher order numerical integration is only necessary when the source point p is located close to the crack surface.

Stress intensity factors at nodes of crack front are calculated using the formulas of Bui [30]:

$$K_I = \frac{v_I E}{8(1-\nu^2)} \sqrt{\frac{2\pi}{d}} \tag{45}$$

$$K_{II} = \frac{v_{II} E}{8(1-\nu^2)} \sqrt{\frac{2\pi}{d}} \tag{46}$$

$$K_{III} = \frac{v_{III} E}{4(1-\nu)} \sqrt{\frac{2\pi}{d}} \tag{47}$$

where v_I is an opening displacement, v_{II} - an in-plane displacement component normal to the crack front, and v_{III} - an in-plane displacement tangent to the crack front. The above displacements are for the nodes closest to the crack front, their distance to the crack front being d.

5.4 Results of Computations Using Original Algorithm

The computational algorithm presented in the preceding section was used to solve the problem of the penny shaped crack under two kinds of loads: constant pressure and constant shear. Three different meshes were used (Figure 28). All the meshes used quarter point element modeling for the displacements close to the crack front (which results in $O(\sqrt{r})$ variation of the displacements as a function of distance r to crack front). It is

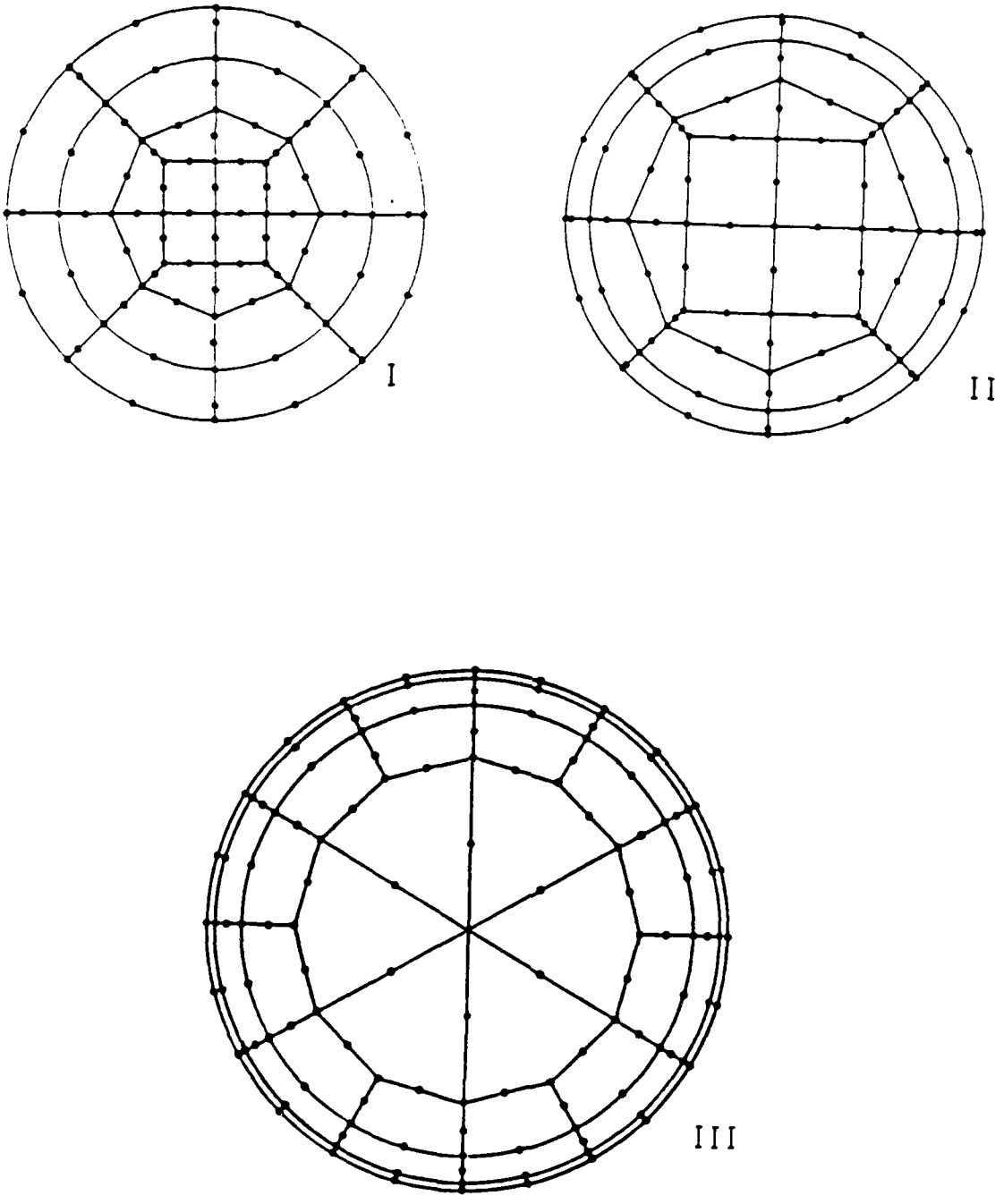

Figure 28. Three Interpolation Meshes Used in the Study

important to point out, though, that the associated displacement gradient M-mesh did not have the $O(\frac{1}{\sqrt{r}})$ singularity. The resulting crack opening displacement patterns in the radial direction along with the exact Sneddon [34] and Segedin [36] solutions are given in Figure 29 (z displacement due to pressure loading) and Figure 30 (x displacement due to xz shear loading).

It is clear from the figures that the results depend very strongly on the mesh used and exhibit a strong oscillatory character. The accuracy of results is clearly unacceptable (17% to 25% error in all stress concentration factors, similar order of magnitude for maximum displacement errors). It is interesting to observe, relatively, that the best results were obtained for the most uniform mesh: the smoothest of the three displacement variations and 17% error in stress concentration factors.

Stresses in the crack plane were calculated for all three solutions. Consistently, they showed the same order of accuracy as the crack opening displacements. Again, the best results were obtained for the uniform mesh; the errors displayed the same behavior as crack opening displacements - the biggest errors were nearest crack front, the smallest away from the crack.

One very clear feature of all results was observed: consistently low displacements and stresses (as compared with exact solutions). The reason for this behavior was ascribed to finite (not zero) compliance of crack front. One way of assuring more physically appropriate behavior of the numerical system was to implement the singularity of displacement gradients in the vicinity of crack front. Intuitive reasoning would suggest this as a way of building in more compliance at the crack front, increasing the overall level of displacements and stresses.

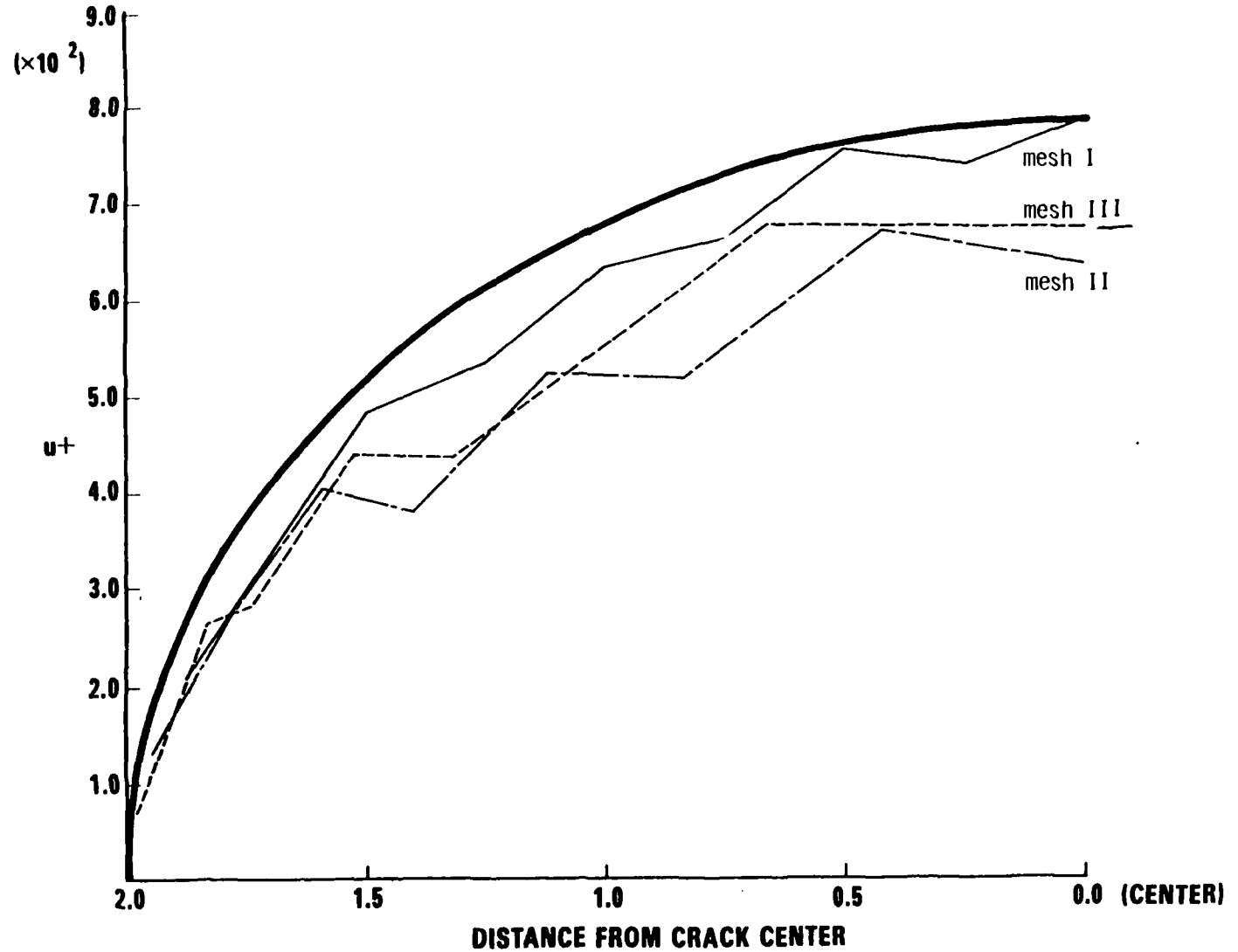

Figure 29. Crack Opening Displacements Due to Pressure Loading

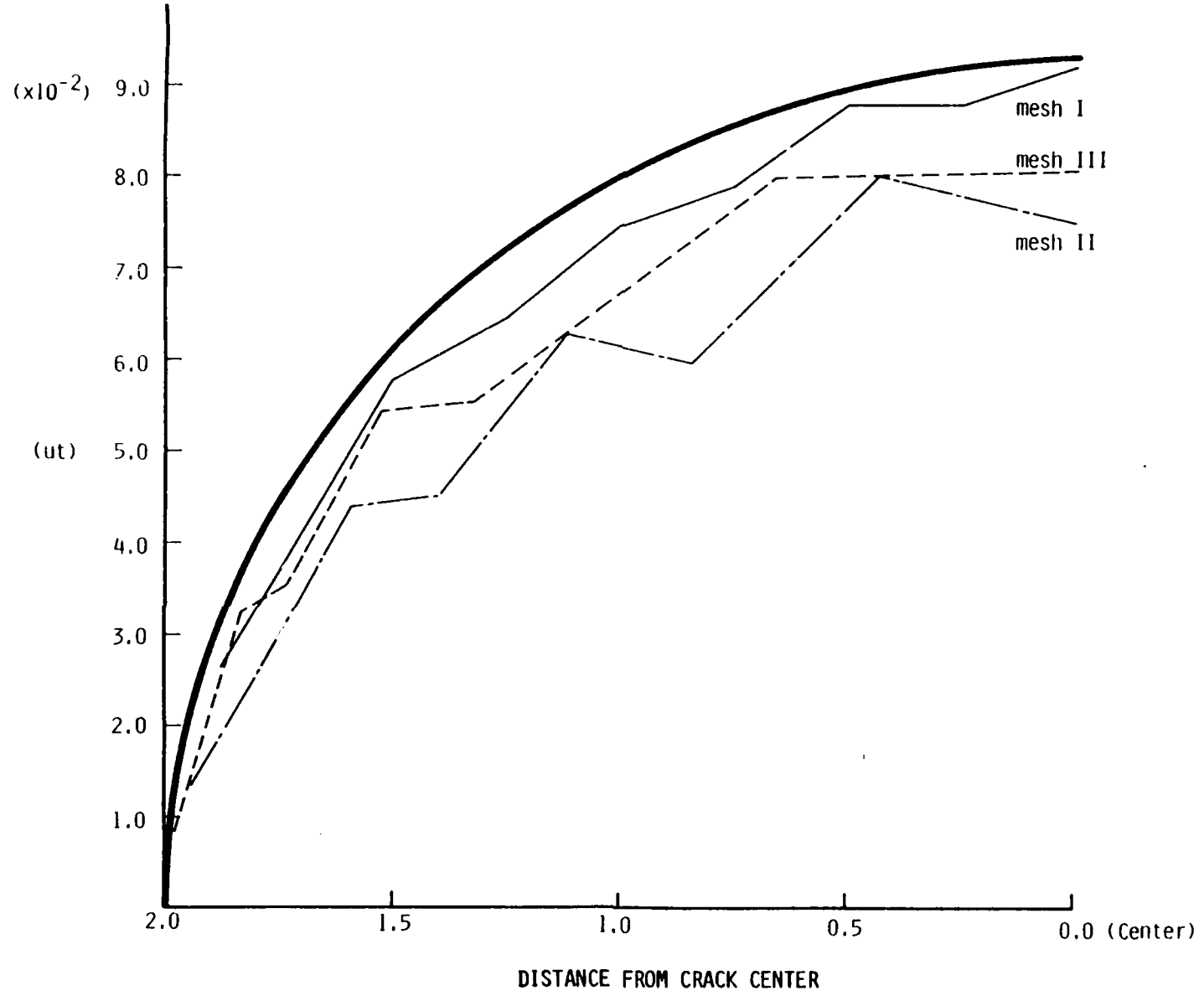

Figure 30. Crack Face Sliding Displacements Due to Shear Loading

5.5 Analysis of Method's Equations Using Exact Solution

Poor results of the method provoked extensive investigations of the sources of errors. The simplest check of the numerical accuracy consisted in the substitution of the obtained displacements into the system (42) and calculation of the right hand sides. It revealed no apparent numerical problem.

Further investigation into the problem used a known (Sneddon [34]) solution for a penny shaped crack to check the accuracy of various matrices used in the numerical method. First, the accuracy of the interpolation matrix MNM was checked by post-multiplying it by exact displacement pattern to obtain "semi-exact" pattern of displacement gradients (48)

$$\{v_{i,\alpha}\}_{s.e.} = [MNM]\{v_i\}_{exact} \tag{48}$$

Comparison of the semi-exact displacement gradients with exact ones predictably showed the biggest errors, on the order of 10%, at the nodes closest to the crack front. Errors at the very boundary were obviously incomparable (the exact solution being infinite while the semi-exact is finite) due to the simple linear displacement gradient assumption used. Errors elsewhere on the crack surface were small (<5%), indicating the adequacy of the displacement gradient model for the regions without singularity. Overall, the results of this test showed the local importance of singularity model of the crack front.

The second test, on the accuracy of traction BIE matrix VV (equation (40)), consisted of substituting both the exact and semi-exact displacement gradient patterns into equation (41) and checking resultant right hand sides. Since the exact solution is infinite on the crack front, a very large

number was used instead for the nodes on the boundary. This test revealed the global importance of crack front singularity as all of the equations displayed very large right hand sides (consistent with the large number used for infinity at the crack front).

Ensuing rigorous analysis of the system of equations (43-43b) proved that in fact the influence of the crack front displacement gradients was present in all of the equations of the system. Even though the equations corresponding to collocation points on the crack boundary were deleted as a part of accounting for boundary conditions, the information about the magnitude of crack front displacement was present throughout the system. The experiment with the semi-exact displacement gradients showed comparable order of errors of right-hand sides as displacement gradients themselves. The most important conclusion of this test was the global importance of crack front singularity modeling.

5.6 Crack Front Singularity Implementation

It is very well known that displacement gradients are singular at the crack front much as the stresses are singular ahead of the crack (order of singularity $0(\frac{1}{\sqrt{r}})$). This kind of singularity may be modeled effectively by so-called quarter-point elements, quadratic isoparametric finite elements with mid-side nodes moved to a quarter side length location. In the current application, these elements may be used only for displacement modeling since the nodal variables for these elements are displacements and the singularity is desired in displacement gradients. For modeling of the displacement gradients, the explicit singularity had to be used in conjunction with slightly modified linear shape functions.

If we consider a one-dimensional quarter point element, the displacement derivative singularity has the form (Henshell and Shaw [36]).

$$\frac{du}{dr} = \frac{A}{\sqrt{r}} + B \tag{49}$$

This expansion allows for very accurate modeling of the displacement gradient pattern resulting from the elliptical displacement distribution. The same variation of displacement gradients was thus assumed for both pairs of 4-noded elements. The resulting shape functions for these elements had the form given in eqs. (50) and (51):

Element adjacent to crack front:

$$M_1(\xi_1\xi_2) = \sqrt{\frac{2}{1+\xi_2}}(1 + \xi_1)(1-\sqrt{\frac{1+\xi_2}{2}})$$

$$M_2(\xi_1\xi_2) = \sqrt{\frac{2}{1+\xi_2}}(1-\xi_1)(1-\sqrt{\frac{1+\xi_2}{2}}) \tag{50}$$

$$M_3(\xi_1\xi_2) = \frac{1}{2}(1-\xi_1)$$

$$M_4(\xi_1\xi_2) = \frac{1}{2}(1+\xi_1)$$

Element of the second row:

$$M_1(\xi_1\xi_2) = \sqrt{\frac{2}{5-3\xi_2}}(1+\xi_1)(1-\frac{1}{2}\sqrt{\frac{5-3\xi_2}{2}})$$

$$M_2(\xi_1\xi_2) = \sqrt{\frac{2}{5-3\xi_2}}(1-\xi_1)(1-\frac{1}{2}\sqrt{\frac{5-3\xi_2}{2}})$$

$$M_3(\xi_1\xi_2) = \frac{1}{2}\sqrt{\frac{2}{5-3\xi_2}}(1-\xi_1)(\sqrt{\frac{5-3\xi_2}{2}} - 1) \tag{51}$$

$$M_4(\xi_1\xi_2) = \frac{1}{2}\sqrt{\frac{2}{5-3\xi_2}}(1+\xi_1)(\sqrt{\frac{5-3\xi_2}{2}} - 1)$$

In the above, an assumption is used that the quarter point elements are employed for the first row of elements adjacent to crack front. Since the shape functions (50) are unbounded and both sets are nonlinear, the standard Galerkin procedure for calculation of nodal displacement gradients was proven to be ineffective and the collocation method was used instead (only on quarter point elements).

The effectiveness of the new, mixed method for displacement gradient interpolation was tested on the mesh of Figure 31. The elliptical displacement pattern was imposed on the nodes of the mesh and the resulting displacement gradients were calculated using standard (non-singular) and new, mixed method. The plots of the results of both methods, along with the exact and unsmoothed N-mesh distributions, are presented in Figure 32. The typical behavior of the interpolation schemes is clearly more visible in Figure 33, where it is shown blown up on two elements closest to the crack front. The results clearly indicate the improved accuracy of displacement gradient modeling of the new mixed method over the previous, linear only method. The deficiency of the standard F.E. modeling of displacement gradients is also obvious from the plot, due to the discontinuities at element boundaries.

Additional improvement in this displacement gradient modeling is offered by the use of transition elements (Labeyrie and Chauchot [37]). The approach is based on focusing the singularities of a few elements, starting from the quarter point element, on a single location, by moving their mid-side nodes to suitable positions (Figure 34). Use of transition elements allows for a better modeling of displacement gradients by N-mesh alone, resulting in a better approximation by M-mesh. Our study of the transition elements showed that the better displacement gradient modeling capability of these elements stems from the presence of the nonlinear term in the geometry mapping.

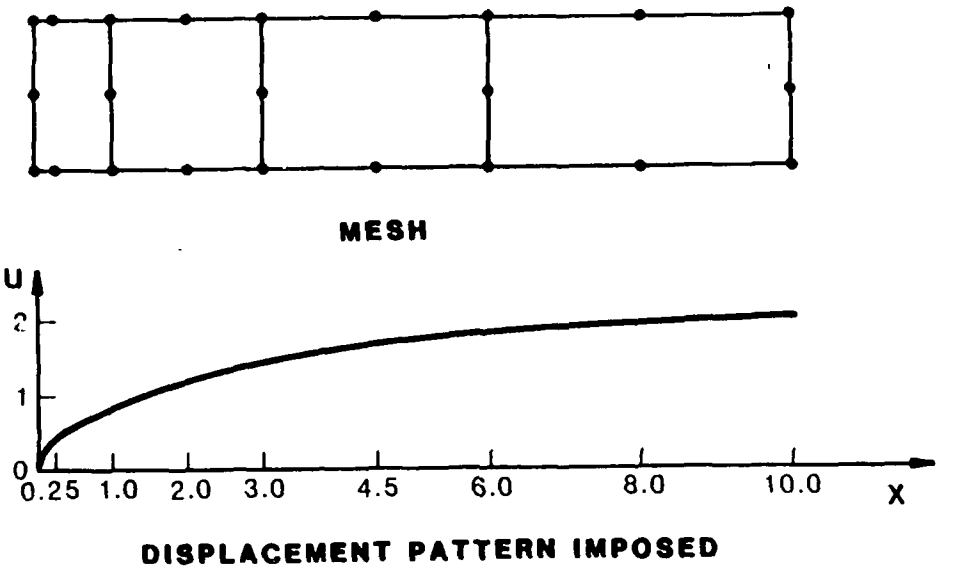

Figure 31. Interpolation Test for 2D Crack Displacement Field

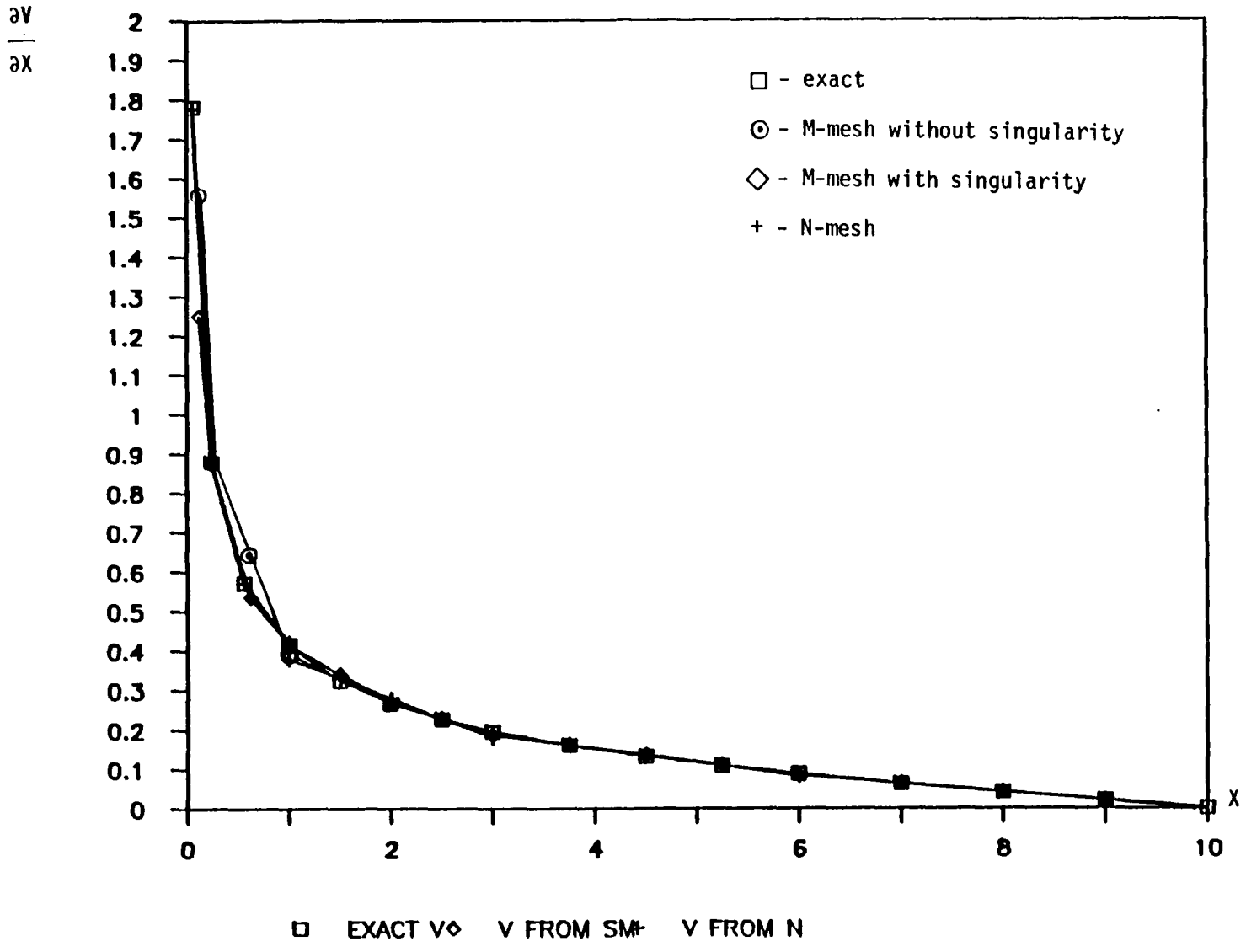

Figure 32. Results of Interpolation by Different Methods

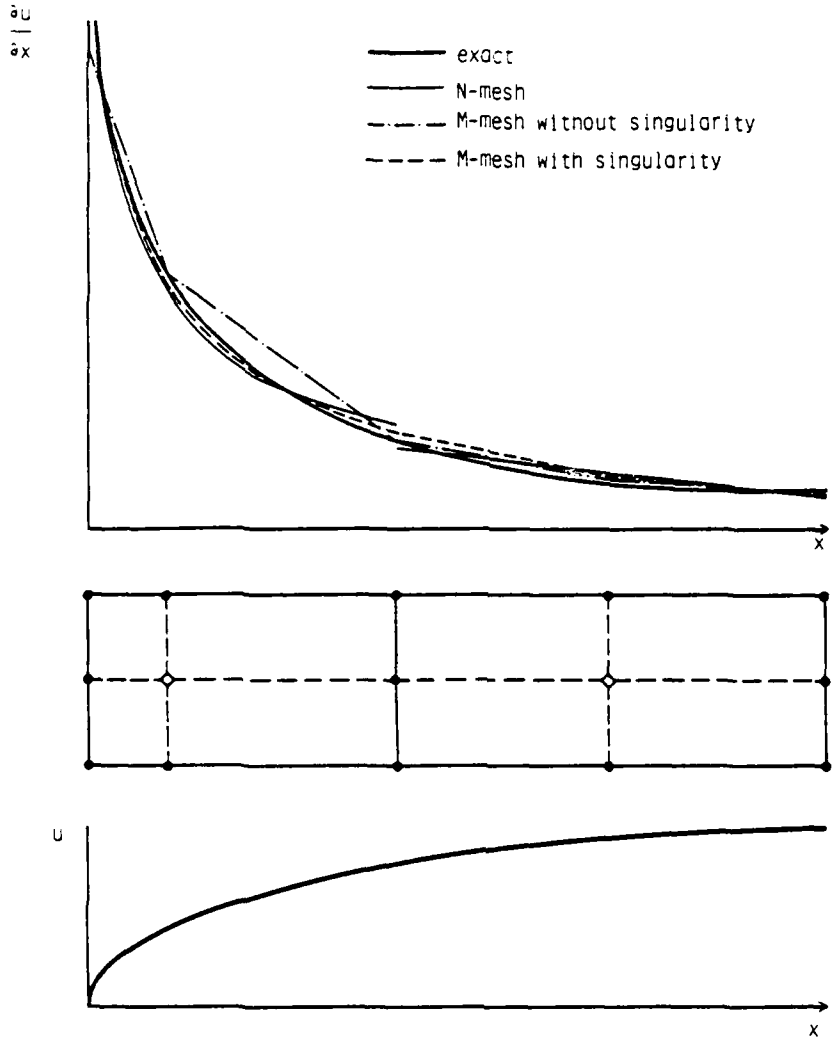

Figure 33. Typical Results of Interpolation by Different Methods

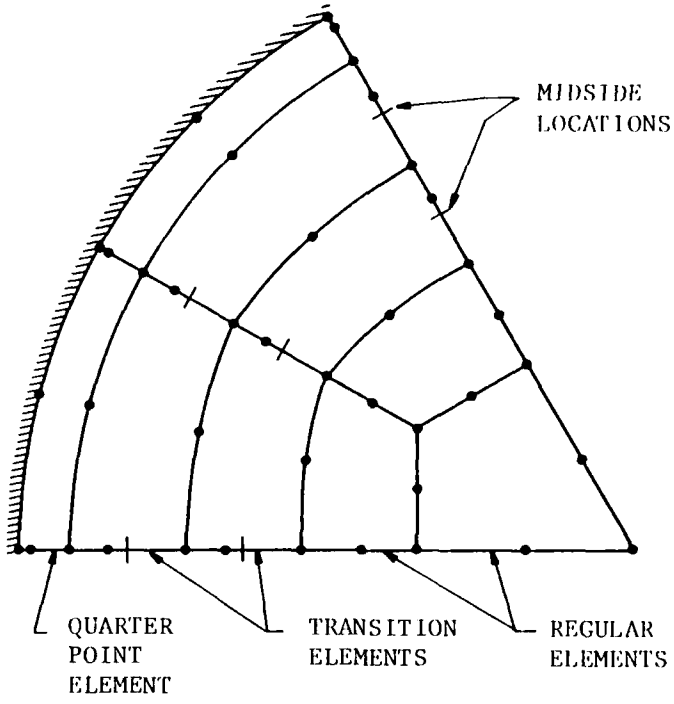

Figure 34. Use of Transition Elements in Crack Front Singularity Modeling

Nonuniformity of geometry mapping allows for nonlinear displacement gradients, enabling a more accurate fitting of the crack front displacement gradient singularity. (Standard, exactly mid-side, quadratic elements map geometry in a linear fashion. As a result, exactly linear variation of displacement gradients is possible).

The results of the computations for the previous model, modified slightly to produce transition elements, are presented on Figure 35. They show important improvements over the previous model (without transition) Figure 32. The basic difference between two N-mesh models is significantly reduced discontinuity of displacement derivatives on element boundaries. Resulting gains in the M-mesh interpolation accuracy reach 50%. The test clearly substantiates the usefulness of transition elements.

The use of the new shape functions for displacement gradient modeling results in a change in the nodal variables for the boundary. Instead of being displacement derivatives at these locations, the new degrees of freedom are actually the coefficients A in the expansion (49):

$$v^{*}_{i,\alpha}{}^{\text{boundary}} = \lim_{r\to 0} \sqrt{r}\ \ v_{i,\alpha}(r) \tag{52}$$

where r is the crack front distance

This property allows for calculation of stress concentration factors from boundary unknowns instead of displacements at quarter point locations

$$K_I = \frac{(V^{*}_{3,1}\cos\theta + V^{*}_{3,2}\sin\theta)}{8(1-\nu^2)}\ \sqrt{2\pi} \tag{53}$$

$$K_{II} = \frac{(V^{*}_{1,1}\cos\theta + V^{*}_{2,2}\sin\theta)}{8(1-\nu^2)}\ \sqrt{2\pi} \tag{54}$$

TRANSITION ELEMENTS

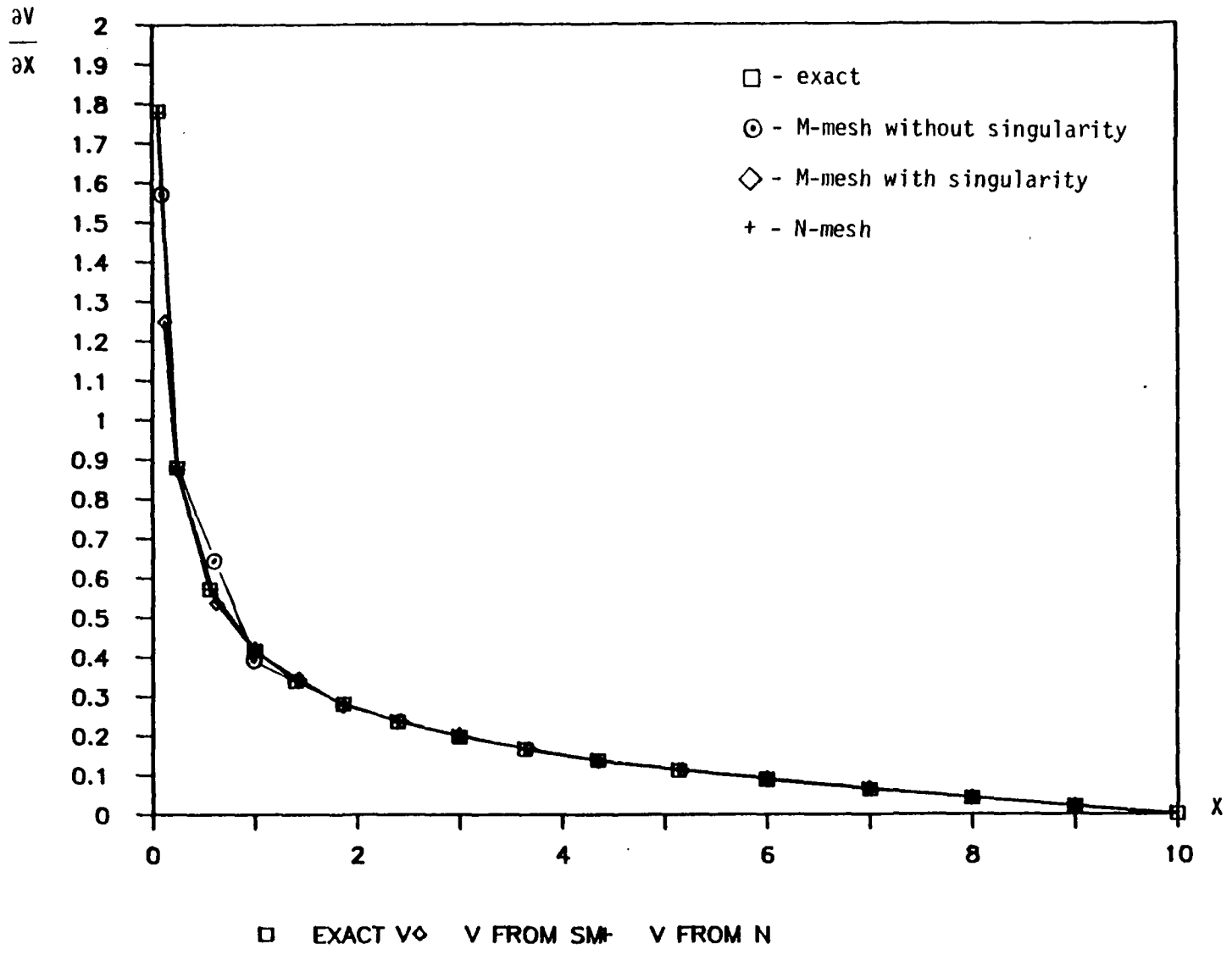

Figure 35. Results of Interpolation by Different Methods Using Transition Elements

$$K_{III} = \frac{(V^*_{2,1}\cos\theta + V^*_{1,2}\sin\theta)}{4(1-\nu)} \sqrt{2\pi} \qquad (55)$$

5.7 Directions of Further Work on Traction BIE

Due to the lack of numerical results for the singularity model in the traction BIE, it is difficult to formulate definitive conclusions. The analysis of the exact solution and the results of the much improved displacement gradient modeling seem to indicate the possibility of substantial gains in the stress intensity factor accuracy. A little less certain is the impact of the singularity on the overall level of displacements. It is difficult to estimate the effect of the singularity on the oscillatory character of displacement results. The use of the collocation method for the formulation of system of equations from the original integral equation may be responsible for this phenomenon. In this case, use of the weighted residual approach (Galerkin scheme) may be necessary to remove the oscillations. The use of the Rayleigh-Ritz procedure (which is normally equivalent to the Galerkin scheme) suggested by Bui (30), in conjunction with singularity modeling, is impossible, due to the appearance of the $(\frac{1}{r})$ term in the four-fold integral resulting from the method. This term will result from two $(\frac{1}{\sqrt{r}})$ terms appearing in explicitly formulated singularities of shape functions.

Further work in the development of the method will require studies in the method's capacity for modeling more complex cases. This capability is essential for the use of the algorithm as a part of alternating method. The more complex loading will probably necessitate the use of Galerkin scheme, since the collocation method carries no information about the interpolation of loads, into the final system of equations. There are also indications, Hanson and Phillips [38], that the Galerkin scheme will yield a more tractable set of equations.

6.0 PROGRAM ACCOMPLISHMENTS AND CONCLUSIONS

The principal goal of the sponsored research was the development and exploitation of the boundary-integral equation method for fracture mechanics analysis of two-dimensional problems with crack tip plasticity. The formulation approach used was quite unique and was based on a special BIE formulation which explicitly accounts for the presence of the crack in satisfying boundary conditions and, for the elastic problem, satisfying the internal equilibrium conditions. Elastoplastic behavior was successfully added to this special fracture mechanics modeling capability with positive benefits in terms of numerical and theoretical results.

New theoretical developments were achieved as a direct result of the use of a BIE formulation approach. Finite element methods begin with an approximation of the total field equations for the problem; BIE does not. Because the BIE formulation makes direct use of relations that satisfy the elastic field behavior, even for the numerical solution results, certain field results are directly and exactly accounted for:

1. The analytical formulation established limits on the strength of the plastic strain increment singularity. In finite element modeling, one can deduce only the limits on strain energy. The BIE result confirmed that the plastic strain increment must satisfy the conditions of singularity previously adduced to plasticity theory, based on nonlinear elastic modeling.

2. The analytical result demonstrated that the plastic singularity behavior derives from a singular eigenvalue problem of a unique form, for the plastic field near the crack tip. At this point, the solution to this singularity formulation is imbedded in the numerical algorithm, as an analytical solution does not seem possible.

3. A new result was achieved for the direct calculation of elastic stress intensity factors for cracks influenced by nonsingular inelastic strains. These problems include residual strain due to welding or elastoplastic notch behavior, thermal strains, etc. The new result shows that extremely accurate stress intensity factor calculations can be made which directly account for these volumetric strain distributions. Published numerical results were generated for plastic notches and for a simplified welding problem.

4. As a result of 3., potentially very important insight has been achieved into the behavior of crack extension into prior plastic zones, due to cyclic loading of the crack. In particular, it was proven analytically and confirmed numerically that the elastic singularity applies for the effect of all prior crack tip plasticity on a crack which has slightly extended into this prior crack tip plasticity. This result explains why certain residual stress retardation models apply to the fatigue crack overload problem. In fact, results obtained using the new code, derived since the close of the current contract, show that the effects of closure and retardation share a dual role on reducing crack driving force; they are essentially two versions of the same phenomenon.

5. The last major analytical result for the 2D problems was the demonstration that the new BIE code could be used as a direct means for calculation of two-dimensional crack weight functions for problems with completely arbitrary geometries, boundary conditions, and internal strain distributions. The new algorithm was demonstrated for several test problems and shows accuracy comparable to the best numerical models available.

6. Finally, the results of the research will appear in several archival journal articles and have been presented in a variety of technical symposia. The following lists the articles and presentations:

AD-A173 216 NONLINEAR FRACTURE MECHANICS ANALYSIS WITH BOUNDARY INTEGRAL METHOD(U) SOUTHWEST RESEARCH INST SAN ANTONIO TX T A CRUSE ET AL. 30 MAY 86 SWRI-06-8044 2/2

UNCLASSIFIED AFOSR-TR-86-0862 F49620-84-C-0042 F/G 20/11 NL

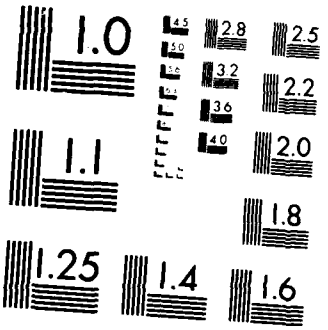

MICROCOPY RESOLUTION TEST CHART
NATIONAL BUREAU OF STANDARDS 1963-A

1. "Fracture Mechanics," T.A. Cruse, Boundary Element Methods in Mechanics, book in series Computational Methods in Mechanics, edited by D.E. Beskos, Elsevier Science Publishers B.V., Amsterdam, to be published.

2. "Elastoplastic BIE Analysis of Cracked Plates and Related Problems, Part 1: Formulation," T.A. Cruse and E.Z.Polch, International Journal for Numerical Methods in Engineering, vol. 23, pp. 429-437 (1986).

3. "Elastoplastic BIE Analysis of Cracked Plates and Related Problems, Part 2: Numerical Results," T.A. Cruse and E.Z. Polch, International Journal for Numerical Methods in Engineering, vol. 23, pp. 439-452 (1986).

4. "Advanced Algorithms for Fracture Mechanics in Two and Three Dimensions," T.A. Cruse and E.Z. Polch, 2nd International Conference on Variational Methods in Engineering, Southampton, England, July 17-19, 1985.

5. "BIE Analysis of Crack Tip Plastic Zones," T.A. Cruse and E.Z. Polch, Proc. of AIAA/ASME/ASCE/AHS 26th Structures, Structural Dynamics, and Materials Conference, Orlando, Florida, April 15-17, 1985, AIAA, New York.

6. "Application of an Elastoplastic Boundary Element Method to Some Fracture Mechanics Problems," T.A. Cruse and E.Z. Polch, Engineering Mechanics, vol. 23, No. 6, pp. 1085-1096 (1986).

7. "A General Solution Procedure for Fracture Mechanics Weight Function Evaluation Based on the Boundary Element Method," T.A. Cruse, submitted to Computational Mechanics: An International Journal.

8. "Buried Crack Analysis with an Advanced Traction BIE Algorithm," E.Z. Polch, T.A. Cruse, and C.-J. Huang, Advanced Topics in Boundary Element Analysis, Ed. by T.A. Cruse, A.B. Pifko, and H. Armen, AMD - Vol. 72, (Proc. of Symposium at ASME Winter Annual Meeting, Miami Beach, Florida, November 17-22, 1985), pp. 173-188, ASME, New York (1985).

The results developed to date are now being used in a systematic study of cyclic crack extension. In particular, these results will be used to guide the modeling and interpretation of data for the current AFOSR sponsored research into small crack behavior, Contract F49620-84-C-0042. It appears clear to us that the behavior of fatigue cracks contains much new information that we are now able to deduce through the unique modeling approach associated with the BIE methodology.

The principal focus of the ongoing work is the interaction of prior plasticity with the current crack driving force. Simplified means for accounting for this interaction are needed in order to do systematic studies

of three-dimensional surface cracks. The insight gained and algorithms developed in the first two year program form a strong basis for the continued study of the fatigue crack growth problem.

REFERENCES

[1] Snyder, M. D., and Cruse, T. A., "Boundary-Integral Equation Analysis of Anisotropic Cracked Plates," International Journal of Fracture, vol. 11, 315-328 (1975).

[2] Cruse, T. A., "Two Dimensional Boundary-Integral Equation Fracture Mechanics Analysis," Applied Mathematics Modeling, vol. 2, 287-292 (1978).

[3] Cruse, T. A., and Polch, E. Z., "Elastoplastic BIE Analysis of Cracked Plates and Related Problems, Part 1: Formulation and Part 2: Numerical Results," International Journal for Numerical Methods in Engineering vol. 23, 429-452 (1986).

[4] Greenberg, M. D., Application of Green's Functions in Science and Engineering, Prentice-Hall, Inc., Englewood Cliffs, New Jersey (1971).

[5] Mukherjee, S., "Corrected Boundary-Integral Equations in Planar Thermoelastoplasticity," International Journal of Solids & Structures, vol. 13, 331-335 (1977).

[6] Hutchinson, J. W., "Singular Behavior at the End of a Tensile Crack in a Hardening Material," Journal of Mechanics and Physics of Solids, vol. 16, 13-31 (1968).

[7] Stern, M., Becker, E. B., and Dunham, R. S., "A Contour Integral Computation of Mixed-Mode Stress Intensity Factors," International Journal of Fracture, vol. 12, 359-368 (1976).

[8] Bathe, K. J., Finite Element Procedures in Engineering Analysis, Prentice-Hall, Inc., Englewood Cliffs, New Jersey (1982).

[9] Haward, R. N., and Owen, D. R. J., "The Yielding of a Two Dimensional Void Assembly in an Organic Glass," Journal of Materials Science, vol. 8, pp. 1136-1144 (1973).

[10] Telles, J. C. F., The Boundary Element Method Applied to Inelastic Problems, Volume 1 in the series Lecture Notes in Engineering, ed. C.A. Brebbia and S.A. Orszag, Springer-Verlag, Berlin (1983).

[11] Larsson, S. G., and Carlsson, A. J., "Influence of Non-Singular Stress Terms and Specimen Geometry on Small-Scale Yielding at Crack Tips in Elastic-Plastic Materials," Journal of the Mechanics and Physics of Solids, vol. 21, pp. 263-277 (1973).

[12] Tada, H., and Paris, P.C., "The Stress Intensity Factor for a Crack Perpendicular to the Welding Bead," International Journal of Fracture, vol. 21, pp. 279-284 (1983).

[13] Grandt, A.F., Jr., and Kullgren, T.E., "Tabulated Stress Intensity Factor Solutions for Flawed Fastener Holes," Engineering Fracture Mechanics, vol. 18, pp. 435-451 (1983).

REFERENCES
(Cont'd)

[14] Chang, J.B., "Prediction of Fatigue Crack Growth at Cold-Worked Fastener Holes," Journal of Aircraft, vol. 14, pp. 903-908 (1977).

[15] Peterson, R.E., Stress Concentration Factors, J. Wiley and Sons, New York, p. 150 (1974).

[16] Rice, J.R., "Some Comments on Elastic Crack-Tip Stress Fields," International Journal of Solids & Structures, vol. 8, 6, pp. 751-758 (1972).

[17] Bueckner, H.F., "Weight Functions for the Notched Bar," Zeitschrift fur Angewandte Mathematik und Mechanik, vol. 51, pp. 97-109 (1971).

[18] Rooke, D.P. and Cartwright, D.J., Compendium of Stress Intensity Factors, Her Majesty's Stationery Office, London (1976).

[19] Besuner, P.M., "The Influence Function Method for Fracture Mechanics and Residual Fatigue Life Analysis of Cracked Components Under Complex Stress Fields," Nuclear Engineering & Design, vol. 43, pp. 115-154, (1977).

[20] Parks, D.M. (1974), "A Stiffness Derivative Finite Element Technique for Determination of Crack Tip Stress Intensity Factors," International Journal of Fracture, vol. 10, pp. 487-502 (1974).

[21] Sha, G.T., and Yang, C-T., "Weight Function Calculations for Mixed-Mode Fracture Problems with the Virtual Crack Extension Technique," Engineering Fracture Mechanics, vol. 21, 6, pp. 1119-1149 (1985).

[22] Paris, P.C., McMeeking, R.M., and Tada, H., "The Weight Function Method for Determining Stress Intensity Factors," Cracks and Fracture, ASTM STP, vol. 601, American Society for Testing and Materials, pp. 471-489 (1976).

[23] Cartwright, D.J., and Rooke, D.P., "An Efficient Boundary Element Model for Calculating Green's Functions in Fracture Mechanics," International Journal of Fracture, vol. 27, pp. R43-R50 (1985).

[24] Grandt, A.F., Jr., "Stress Intensity Factors for Some Through-Cracked Fastener Holes," International Journal of Fracture, vol. 11, 2, pp. 283-294, (1975).

[25] Petroski, H.J., and Achenbach, J.D., "Computation of the Weight Functions from a Stress Intensity Factor," Engineering Fracture Mechanics, vol. 10, pp. 257-266 (1978).

[26] Bortman, Y., and Banks-Sills, L., "An Extended Weight Function Method for Mixed-Mode Elastic Crack Analysis," Journal of Applied Mechanics, vol. 50, pp. 907-909 (1983).

REFERENCES
(Cont'd)

[27] Cruse, T.A., "Boundary-Integral Equation Method for Three-dimensional Elastic Fracture Mechanics Analysis," AFOSR-TR-75-0813, Accession No. ADA-11060, pp. 13-20 (1975).

[28] Nishioka, T., and Atluri, S.N., "Analytical Solution for Embedded Elliptical Cracks, and Finite Element Alternating Method for Elliptical Surface Cracks, Subjected to Arbitrary Loadings," Engineering Fracture Mechanics, vol. 1, No. 3, pp. 247-268 (1983).

[29] Weaver, J., "Three-Dimensional Crack Analysis," International Journal of Solids and Structures, vol. 13, pp. 321-330 (1977).

[30] Bui, H.D., "An Integral Equation Method for Solving the Problem of Plane Crack of Arbitrary Shape," J. Mech. Phys. Solids, vol. 25, pp. 23-39 (1977).

[31] Putot, C.J., "Une Nouvelle Methode d' Equations Integrales pour Certains Problemes de Fissures Planes," These, Universite Paris VI (1980).

[32] Hinton, E., and Campbell, J.S., "Local and Global Smoothing of Discontinuous Finite Element Functions Using a Least Squares Method," Int. J. Numerical Methods in Engineering, vol. 8, pp. 461-480 (1974).

[33] Cruse, T.A., "Numerical Solutions in Three-Dimensional Elastostatics," Int. J. Solids and Structures, vol. 5, pp. 1259-1274 (1963).

[34] Sneddon, I.N., Proc. Royal Society (London) Ser. A. vol. 187, pp. 229 (1946).

[35] Segedin, C.M., "Note On a Penny-Shaped Crack Under Shear," Proc. of the Cambridge Philosophical Society, vol. 47, pp. 396-400 (1950).

[36] Henshell, R.D., and Shaw, K.G., "Crack Tip Elements Are Unnecessary," Int. J. Numerical Methods in Engineering, vol. 9, pp. 495-509 (1975).

[37] Labeyrie, J., and Chauchot, P., "On the Crack Tip Singularities In 3-D BEM," Boundary Elements VI, Proc. of the 6th International Conference, on board the liner The Queen Elizabeth 2, Southampton to New York, Springer Verlag, (1984).

[38] Hanson, R.J., and Phillips, J.L., "Numerical Solution of Two-Dimensional Integral Equations Using Linear Elements," SIAM J. Numerical Analysis, vol. 15, No. 1, pp. 113-121 (1978).

END

12-86

DTIC